Struct Chem
DOI 10.1007/s11224-015-0704-7

ORIGINAL RESEARCH

The structure of β-diketones related to curcumin determined by X-ray crystallography, NMR (solution and solid state) and theoretical calculations

Carla I. Nieto[1] · Pilar Cabildo[1] · Rosa M. Claramunt[1] · Pilar Cornago[1] · Dionisia Sanz[1] · M. Carmen Torralba[2] · M. Rosario Torres[3] · Marta B. Ferraro[4] · Ibon Alkorta[5] · Marta Marín-Luna[5] · José Elguero[5]

Received: 13 October 2015 / Accepted: 12 November 2015

Abstract Structural data are reported on sixteen ketoenols of β-diketones: solution NMR, solid-state NMR (CPMAS and MAS) and X-ray crystallography (four compounds, where three are new). The emphasis is on the tautomerism between both ketoenols, in solution and in the solid state. GIAO/B3LYP/6-311++G(d,p) and Quantum ESPRESSO (QE) calculations were used and compared. For average values, the GIAO/DMSO-PCM is enough, but splittings can only be approached by using QE. A case of rotational disorder has been analyzed. Some anomalies related to C–F bonds and to the C–CF_3 group have been detected.

Keywords Tautomerism · β-Diketones · ^{13}C and ^{19}F NMR · Solid-state NMR · GIAO calculations · Quantum ESPRESSO calculations

Introduction

Few simple compounds of natural origin have originated such a large widespread of patents, original publications and reviews as curcumin (**1**); for this reason, only some recent ones will be cited from other groups [1–7] and from ours [8–10]. Curcumin (**1**) is a β-diketone that owing to its symmetry only has two tautomers, the ketoenol **a** and the diketone **c** (Fig. 1), and the third one, **1b**, being identical to **1a**.

The non-symmetric hemicurcuminoids have three tautomers (Fig. 2), although only the enol ones, **a** and **b**, have been observed.

In the present work, we will discuss twelve compounds: six of the $R = C_6H_5$ series and six of the $R = CF_3$ series, represented below in their **a** tautomeric form (Fig. 3).

In addition, a complete study of their NMR properties in solution and in the solid state, the X-ray structures of four compounds will be discussed, one already published **8** [10] (CCD refcode: UFIMON [11–13]), and three new: **5**, **7** and **9**.

In our two previous papers, some properties of compounds **2** [8, 10], **3**, **4** and **8** [10] were reported. Besides, four other curcuminoids necessary for the discussion were described: **14** [8, 10]), **15** [8], **16** [8] and **17** [8] (Fig. 4). The X-ray structures of **2**, **3**, **4**, **8** and **14** were already reported [10].

Electronic supplementary material The online version of this article (doi:10.1007/s11224-015-0704-7) contains supplementary material, which is available to authorized users.

✉ Ibon Alkorta
ibon@iqm.csic.es

Rosa M. Claramunt
rclaramunt@ccia.uned.es

Marta B. Ferraro
ferraro@df.uba.ar

[1] Departamento de Química Orgánica y Bio-Orgánica, Facultad de Ciencias, UNED, Paseo Senda del Rey, 9, 28040 Madrid, Spain

[2] Departamento de Química Inorgánica I, Facultad de Ciencias Químicas, Universidad Complutense de Madrid (UCM), 28040 Madrid, Spain

[3] CAI de Difracción de Rayos-X, Facultad de Ciencias Químicas, Universidad Complutense de Madrid (UCM), 28040 Madrid, Spain

[4] Departamento de Física, Facultad de Ciencias Exactas y Naturales, Universidad de Buenos Aires, and IFIBA, CONICET, Ciudad Universitaria. Pab. I, 1428 Buenos Aires, Argentina

[5] Instituto de Química Médica, Centro de Química Orgánica "Manuel Lora-Tamayo", CSIC, Juan de la Cierva, 3, 28006 Madrid, Spain

Published online: 09 December 2015

Fig. 1 Curcumin tautomers

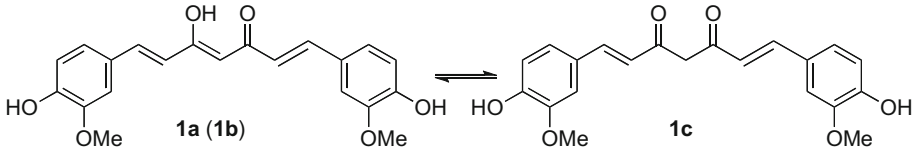

Fig. 2 Three tautomers of hemicurcuminoids

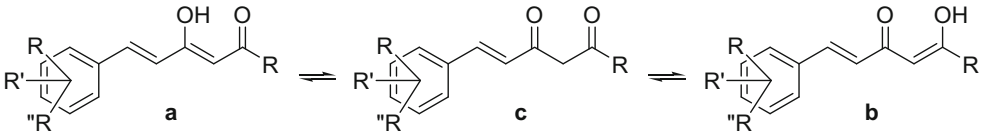

Fig. 3 Twelve hemicurcuminoids

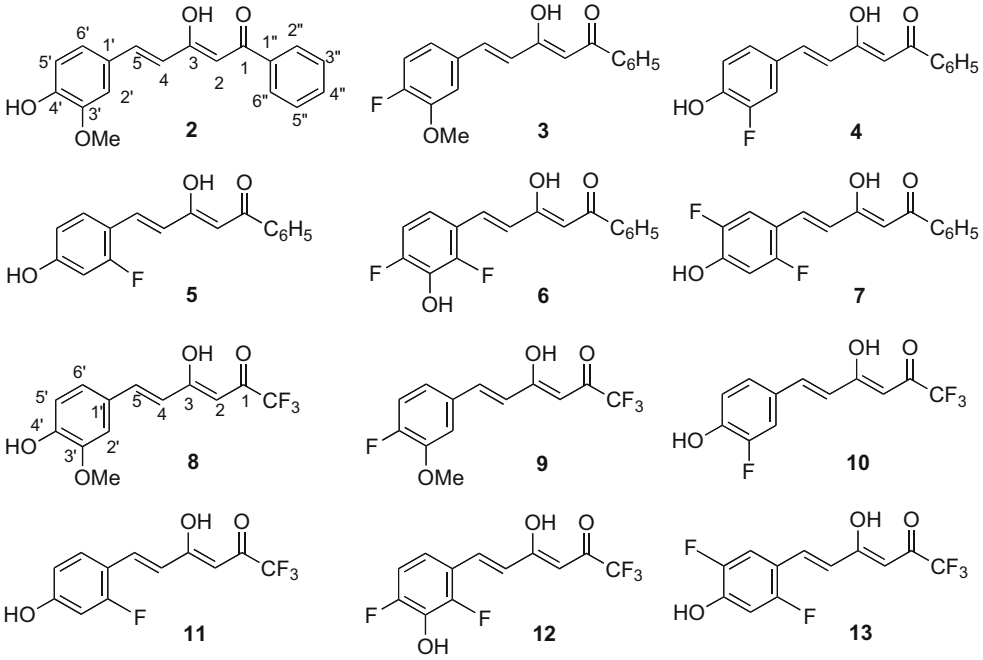

Fig. 4 Four additional hemicurcuminoids

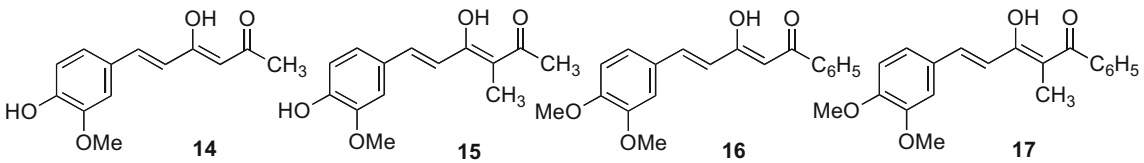

Results and discussion

Energies

We will start by discussing the energy calculations of tautomers **a** and **b** of ketoenols **2**–**17**. The results are reported in Table 1. Compound **5a** has the F atom at position 2', while compound **5a**′ has it at position 6' which corresponds to a rotation about the C5–C1′ bond. The corresponding rotamers for the other tautomers, **5b**′ and **5c**′, were also calculated. For compounds **6** and **12**, OH/Fi means the H of the OH pointing toward Fi, $i = 2'$, $4'$ (Fig. 5).

In the cases where we have calculated the diketo tautomers **c**, they are much less stable (e.g., **5c**, +27.8 kJ mol^{-1}; **8c**, +38.2 kJ mol^{-1}); for this reason, we did not extend such calculations to the remaining compounds. Between **5a** and **5a**′, there is a difference of 1.7 kJ mol^{-1}; at 298.15 K, this corresponds to 66.5 % of **5a** and 33.5 % of **5a**′.

Table 1 Absolute (hartrees) and relative (kJ mol^{-1}) energies (including ZPE) of hemicurcuminoids; dipole moments in D [all calculated at the B3LYP/6-311 ++G(d,p) level]

Comp	P. G.	SCF energy	ZPE	Total energy	Dipole	E_{rel} (kJ mol^{-1})
2a	C_1	−996.71071	0.29919	−996.41152	2.56	0.0
2b	C_1	−996.70926	0.29901	−996.41025	1.67	3.8
3a	C_1	−1020.72331	0.28652	−1020.43678	1.27	0.0
3b	C_1	−1020.72180	0.28632	−1020.43548	1.81	3.9
4a	C_1	−981.41884	0.25851	−981.16033	3.18	0.0
4b	C_1	−981.41737	0.25829	−981.15908	3.21	3.9
5a	C_1	−981.41938	0.25855	−981.16084	4.42	0.0
5a′	C_1	−981.41785	0.25827	−981.16047	6.31	1.7
5b	C_1	−981.41785	0.25830	−981.15955	4.08	4.0
5b′	C_1	−981.41706	0.25800	−981.15907	6.27	6.1
5c	C_1	−981.40878	0.25792	−981.15086	2.53	27.8
5c′	C_1	−981.40937	0.25780	−981.15157	3.25	26.3
6a OH/F4′	C_1	−1080.67926	0.25058	−1080.42868	2.27	0.0[a]
6b OH/F4′	C_1	−1080.67772	0.25034	−1080.42738	1.81	4.1
6a OH/F2′	C_1	−1080.67928	0.25062	−1080.42866	2.18	0.0[a]
6b OH/F2′	C_1	−1080.67778	0.25038	−1080.42739	2.75	3.9
7a	C_1	−1080.68475	0.25049	−1080.43426	2.58	0.0
7b	C_1	−1080.68326	0.25027	−1080.43299	2.29	3.9
8a	C_1	−1102.73993	0.22313	−1102.51680	7.48	0.0
8b	C_s	−1102.73658	0.22279	−1102.51379	6.70	8.8
8c	C_1	−1102.72539	0.22205	−1102.50334	4.50	38.2
9a	C_1	−1126.74883	0.21003	−1126.53879	6.52	0.0
9b	C_1	−1126.74557	0.20967	−1126.53590	5.57	8.5
10a	C_1	−1087.44711	0.18246	−1087.26465	6.28	0.0
10b	C_1	−1087.44389	0.18210	−1087.26178	5.32	8.5
11a	C_1	−1087.44755	0.18252	−1087.26503	8.02	0.0
11b	C_1	−1087.44428	0.18211	−1087.26217	7.09	8.6
12a OH/F4	C_1	−1186.70645	0.17452	−1186.53194	6.84	0.0
12b OH/F4	C_1	−1186.70326	0.17416	−1186.52910	5.86	8.4
12a OH/F2	C_1	−1186.70642	0.17455	−1186.53187	4.32	0.0[b]
12b OH/F2	C_1	−1186.70332	0.17415	−1186.52917	3.39	8.2
13a	C_1	−1186.71224	0.17441	−1186.53783	6.76	0.0
13b	C_1	−1186.70913	0.17394	−1186.53519	5.78	8.2
14a	C_1	−804.92773	0.24559	−804.68214	3.16	0.0
14b	C_1	−804.92710	0.24583	−804.68127	2.04	1.7
15a	C_1	−844.24719	0.27332	−843.97388	2.51	0.0
15b	C_1	−844.24571	0.27302	−843.97269	2.01	3.9
16a	C_1	−1036.00972	0.32665	−1035.68307	2.64	0.0
16b	C_1	−1036.00820	0.32643	−1035.68177	2.07	4.0
17a	C_1	−1075.32487	0.35421	−1074.97077	2.72	0.0
17b	C_1	−1075.32412	0.35420	−1074.96992	2.44	2.0

[a] Actually, the OH/F2′ is 0.04 kJ mol^{-1} less stable than the OH/F4′

[b] Actual value, 0.08 kJ mol^{-1}

To analyze E_{rel} (kJ mol^{-1}), we have used a Free–Wilson (or presence–absence) matrix [14–16] (Table 2). We intend to quantify the substituent effects according to their position. Compounds **6** and **12** present rotational isomerism involving the OH group at position 3′ (Fig. 5): Energetically, both isomers are nearly identical, and we have used the mean value.

A statistical analysis of Table 2, in what concerns the **b**–**a** values defined as the difference in energy between the **b** tautomer and the **a** tautomer (**a** is always the most stable),

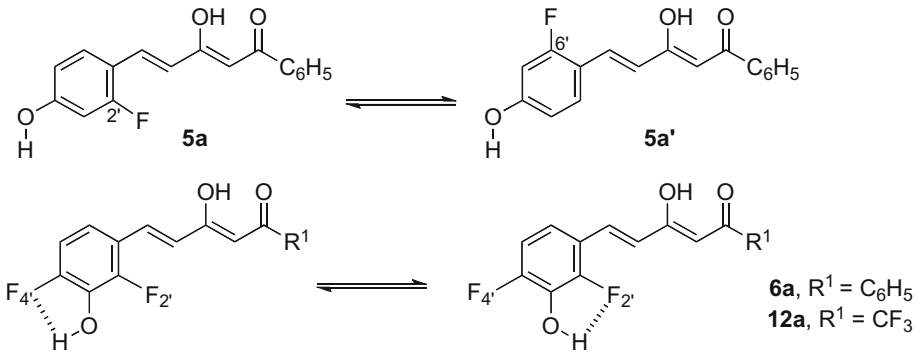

Fig. 5 Rotamers involving the F atom in compound **5a** and the 3′-OH group in compounds **6a** and **12a**

Table 2 Free–Wilson matrix

	$R^1 = C_6H_5$	$R^1 = CF_3$	$R^1 = CH_3$	$R^2 = CH_3$	2′-F	3′-OMe	3′-F	3′-OH	4′-OMe	4′-F	4′-OH	5′-F	**b–a** kJ mol^{-1}
2	1	0	0	0	0	1	0	0	0	0	1	0	3.8
3	1	0	0	0	0	1	0	0	0	1	0	0	3.9
4	1	0	0	0	0	0	1	0	0	0	1	0	3.9
5	1	0	0	0	1	0	0	0	0	0	1	0	4.0
6	1	0	0	0	1	0	0	1	0	1	0	0	4.0
7	1	0	0	0	1	0	0	0	0	0	1	1	3.9
8	0	1	0	0	0	1	0	0	0	0	1	0	8.8
9	0	1	0	0	0	1	0	0	0	1	0	0	8.5
10	0	1	0	0	0	0	1	0	0	0	1	0	8.5
11	0	1	0	0	1	0	0	0	0	0	1	0	8.6
12	0	1	0	0	1	0	0	1	0	1	0	0	8.3
13	0	1	0	0	1	0	0	0	0	0	1	1	8.2
14	0	0	1	0	0	1	0	0	0	0	1	0	1.7
15	0	0	1	1	0	1	0	0	0	0	1	0	3.9
16	1	0	0	0	0	1	0	0	1	0	0	0	4.0
17	1	0	0	1	0	1	0	0	1	0	0	0	2.0

yields significant effects all of them positive ($n = 16$, $R^2 = 0.992$), i.e., all destabilize the **b** tautomer:

$$R^1 = \text{Ph}, +1.2,\ R^1 = CF_3,\ +5.7\ (\text{both with regard to } R^1 = \text{Me}, 0.0 \text{ by definition}),\ 2' - \text{F} + 1.8,\ 3' - \text{OMe} + 1.8,\ 3' - \text{F} + 1.8,\ 4' - \text{F} + 1.0 \text{ and } 4' - \text{OH} + 1.0 \text{ kJ mol}^{-1}\ (\text{both with regard to } R^{4'} = \text{OMe}, 0.0 \text{ by definition}) \quad (1)$$

Crystal structure of hemicurcuminoids 5, 7 and 9

Compounds **5** and **7** crystallize in $Pna2_1$ orthorhombic space group; meanwhile, **9** do it in $P2_1/n$ monoclinic space group. Figures 6, 7 and 8 display ORTEP plots for compounds **5**, **7** and **9**, showing the labeling of their asymmetric units.

Compounds **5** and **7** present one single molecule per asymmetric unit which is, as expected, almost planar. The maximum dihedral angle between the phenyl ring and the rest of the molecule is 4.7(4)° for **5** and 6.6(4)° for **7**. In contrast, compound **9** contains two crystallographically different and independent molecules per asymmetric unit, named A and B, due to the diverse interactions that each type of molecule presents. Both molecules are slightly more deviated from planarity than in **5** and **7**, being their maximum dihedral angles of 9.1(3)° and 11.6(3) in A and B, respectively. The planarity of the molecules in the three compounds is in good agreement with the extended electronic delocalization supported by the experimental bond distances.

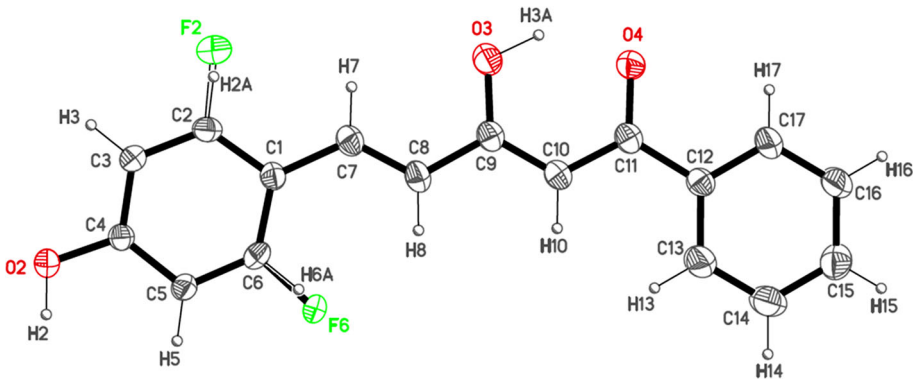

Fig. 6 ORTEP plot of **5** (20 % probability for the ellipsoids) showing the labeling of the asymmetric unit. In this compound, the F atom is disordered, 70 % on C6 and 30 % on C2

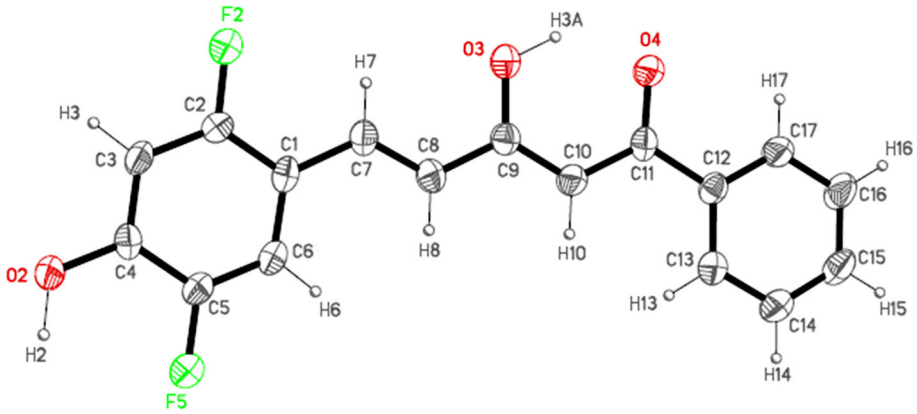

Fig. 7 ORTEP plot of **7** (30 % probability for the ellipsoids) showing the labeling of the asymmetric unit

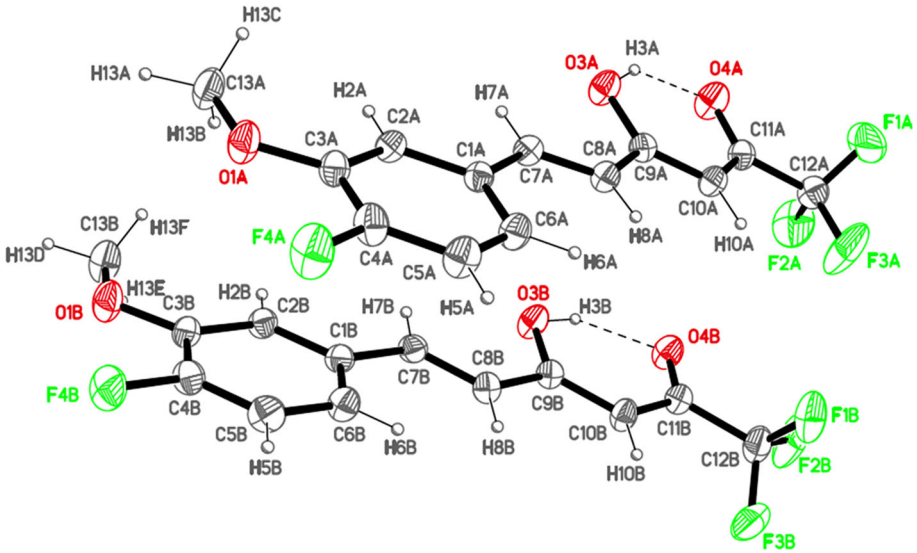

Fig. 8 ORTEP plot of **9** (20 % probability for the ellipsoids) showing the labeling of the asymmetric unit

In concordance with our previous results [8, 10], all the molecules are in the β-ketoenol tautomeric form. From the crystal data, it can also be deduced that tautomer **a** (O3–H3) predominates since the C11–O4 distances, found in the range 1.240–1.282(5) Å, indicate a higher bond order, while the C9–O3 ones, 1.315–1.333(5) Å, are longer.

An intramolecular hydrogen bond between O3H3···O4 atoms in the three derivatives is also observed. This interaction is similar in **7** and **9** but shorter in **5**, but the extent of symmetrization is equivalent in all of them. The hydrogen bonding distances and angles for **5**, **7** and **9** are listed in Table 3.

Table 3 Hydrogen bonds (Å and °) for **5**, **7** and **9**

Compound	D–H···A	Symmetry operations	*d*(D–H)	*d*(H···A)	*d*(D···A)	<(DHA)
5	O3–H3A···O4		0.99	1.71	2.530(4)	137.0
	O2–H2···O4#1	#1 −x + 1/2, y + 1/2, z + 3/2	1.20	1.54	2.716(4)	166.9
7	O3–H3···O4		1.00	1.73	2.517(4)	132.9
	O2–H2···O4#1	#1 −x + 3/2, y − 1/2, z + 3/2	1.00	1.72	2.711(4)	169.0
9	O3A–H3A…O4A		1.02	1.73	2.582(3)	138.4
	O3B–H3B…O4B		1.06	1.70	2.560(3)	134.5

Along with the intramolecular hydrogen bonds already described, **5** and **7** present intermolecular hydrogen bonds between the phenol group and the carbonyl oxygen of an adjacent molecule (O2H2···O4#1; Table 3). Besides, in compound **7** the *ortho* position of F5 relative to phenol allows the formation of an additional interaction with the enol hydrogen of a neighboring molecule [distance O3H3···F5#1 of 2.448(5) Å]. This double interaction can be related to the longer H3A···O4 distance compared to that for compound **5** where only the interaction with the phenol exists.

These intermolecular hydrogen bonds between adjacent coplanar molecules lead to the formation of zigzag chains as it can be seen in Figs. 9 and 10. The chains are isolated as no significant additional interactions are found between them.

Compound **9**, however, displays a different packing due to its two non-equivalent molecules (Fig. 11). Thus, type A molecules are interconnected through the fluorine atom F4A that are hydrogen-bonded to H10A atom of neighboring molecules, because of its acidic character, giving rise to chains with the molecules zigzagged with an angle of 33.4(3)° between them.

On the other hand, every type B molecule interacts only with one coplanar type A through two asymmetric contacts between H3A···O3B (2.303(2) Å) and H3B···O3A [2.672(2) Å]. To the former, being shorter corresponds to an intramolecular hydrogen bond, O3B–H3B···O4B, stronger than the analogous in type A molecules (Table 3).

NMR spectroscopy of hemicurcuminoids 2–13

The experimental NMR results (chemical shifts in ppm, spin–spin coupling constants, SSCC, in Hz) necessary for the discussion are reported in Tables 4, 5, 6, 7, 8 and 9.

The ^{19}F chemical shifts of the trifluoromethyl groups, both in solution and in the solid state, appear between −73.4 and −77.7 ppm (Table 9), values typical of the ketoenol tautomers (that of the diketo tautomer resonates at −80/−83 ppm [17]).

From the experimental chemical shifts (δ, ppm) in solution (Tables 4, 5, 6, 7, 8 and 9) and from the GIAO calculated ones (Table S1 of the Appendix A. Supplementary material), we have determined the populations of **a** and **b** tautomers:

$$\delta_{\text{exp}} = \delta\mathbf{a} * \text{pop.}\mathbf{a} + \delta\mathbf{b} * \text{ pop.}\mathbf{b} \quad (2)$$

Although no restraint has been applied, it is worth noting that pop.

$$\text{pop.}\mathbf{a} + \text{ pop.}\mathbf{b} \approx 1 \quad (3)$$

In turn, these populations have permitted to obtain first the equilibrium constant *K*, defined as **b/a**, and then ΔG (298.15 K) (kJ mol^{-1}).

In the case of compounds **6** and **12**, we have compared the experimental chemical shifts to those calculated for the rotamer O–H···F4′ and O–H···F2′ (Fig. 5). The agreement is better for the last rotamer, and the values of Table 10 correspond to it.

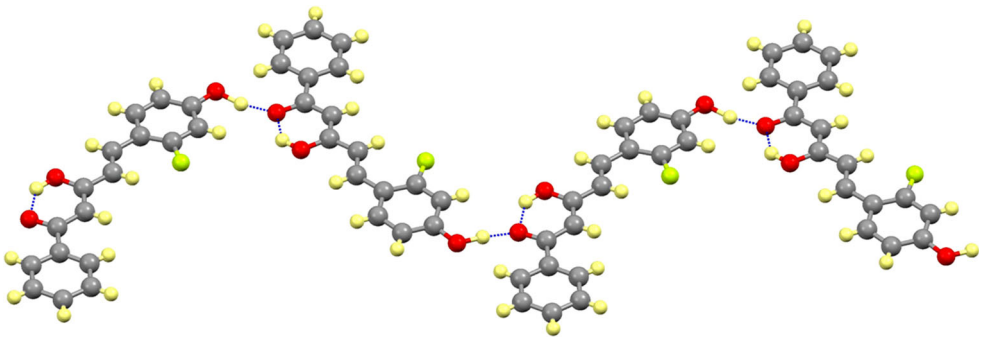

Fig. 9 View of a chain formed by H-bonds in **5** (F atoms disordered over C2 position are omitted for clarity)

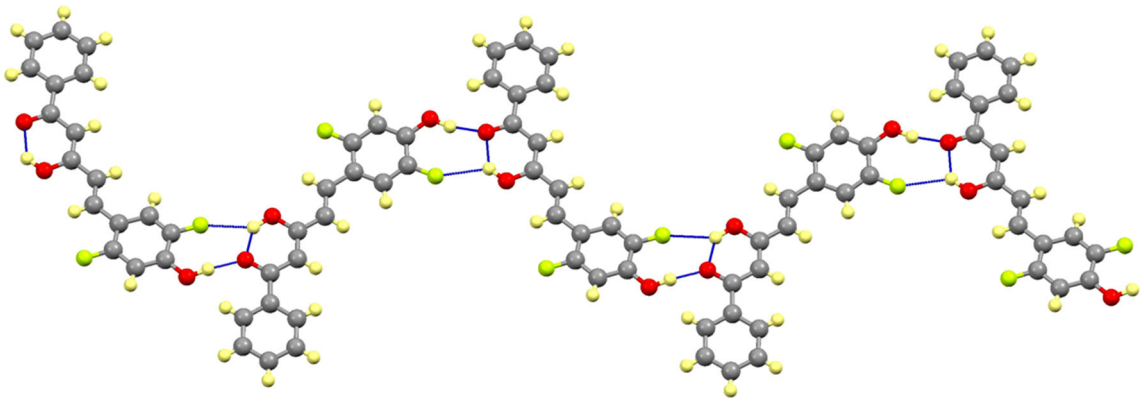

Fig. 10 View of a chain formed by H-bonds in **7**

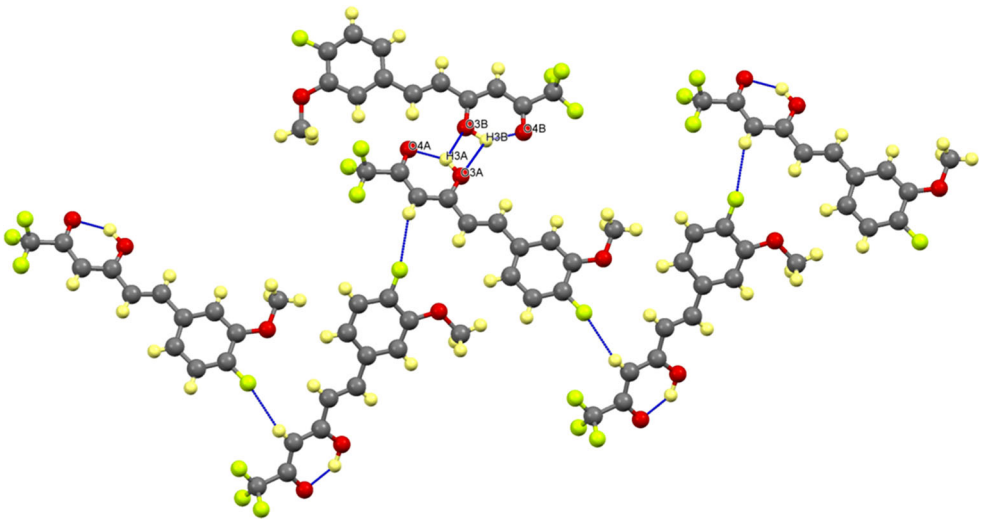

Fig. 11 View of the different interactions between A and B type molecules in **9**

Table 10 indicates that always tautomer **a** predominates although it varies from 53 to 86 %. ΔG is very poorly related to E_{rel}:

$$\Delta G = (2.1 \pm 0.6) + (0.2 \pm 0.1)\, E_{rel}, \quad n = 16, R^2 = 0.31 \tag{4}$$

but it should be noted that E_{rel} corresponds to isolated molecules in the gas phase, while ΔG corresponds to values determined in solution in different solvents (no improvement results by adding dummy variables to represent the different solvents). A Free–Wilson analysis [14–16] of ΔG values was also unsuccessful:

$$\Delta G = (4.1 \pm 0.3) - (1.2 \pm 0.5)\ C_6H_5, \quad n = 16, R^2 = 0.34 \tag{5}$$

(the CH_3 group was used as reference; the effect of the CF_3 is not significant nor the differences between $CDCl_3$ and DMSO-d_6).

Concerning the rotamers **5a** and **5a′**, a regression with the data of Table 11 leads to the following equation:

$$\delta(\text{DMSO - } d_6) = (0.32 \pm 0.18)\mathbf{5a} + (0.68 \pm 0.18)\mathbf{5a\prime}, \quad n = 18,\ R^2 = 1.000 \tag{6}$$

meaning that in this solvent rotamer **5a′** predominates even if it is less stable that **5a** (Table 1) may be because its dipole moment (6.31 D) is higher than that of **5a** (4.42 D, Table 1).

Solid-state NMR study of hemicurcuminoids 3, 5, 7 and 9

Assuming that only one tautomer is present in the solid state (the splitting of the signals does not correspond to tautomerism as it should be particularly apparent in carbon atoms C1 and C3, which are never split), we have carried out a single regression between the experimental chemical shifts and the calculated ones: in all cases, the square correlation coefficient is larger for tautomer **a** than for tautomer **b** (see Table S1 of the Appendix A). Table 10

Table 4 ^{1}H NMR data of compounds **2–7**

	2[a] $CDCl_3$	**3**[a] $CDCl_3$	**4**[a] $CDCl_3$	**4**[a] DMSO-d_6	**5** DMSO-d_6	**6** DMSO-d_6	**7** DMSO-d_6
H2	6.33 (s)	6.34 (s)	6.32 (s)	6.71 (s)	6.75 (s)	6.82 (s)	6.72 (s)
OH-enol	16.26 (s)	16.1 (br)	16.14 (br)	16.37 (br)	16.30 (br)	16.10 (br)	16.25 (br)
H4	6.52 (d) $^{3}J_{H5} = 15.8$	6.55 (d) $^{3}J_{H5} = 15.8$	6.50 (d) $^{3}J_{H5} = 15.9$	6.82 (d) $^{3}J_{H5} = 15.9$	6.82 (d) $^{3}J_{H5} = 16.1$	6.97 (d) $^{3}J_{H5} = 16.1$	6.89 (d) $^{3}J_{H5} = 16.0$
H5	7.63 (d)	7.55 (d)	7.58 (d)	7.65–7.53	7.65 (d)	7.64 (d)	7.59 (dd) $^{5}J_{F5'} = 1.1$[b]
H2′	7.07 (d) $^{4}J_{H6'} = 1.9$	7.06–7.15	7.58–7.53	7.65–7.53	–	–	–
H3′	3.95 (s) (OCH_3)	3.94 (s) (OCH_3)	–	–	6.65 (dd) $^{4}J_{H5'} = 2.3$ $^{3}J_{F2'} = 12.8$	–	6.83 (dd) $^{3}J_{F2'} = 12.8$ $^{4}J_{F5'} = 7.4$
OH	5.86 (s)	–	5.39 (s)	10.48 (s)	10.55 (s)	10.46 (s)	11.05 (s)
H5′	6.94 (d) $^{3}J_{H6'} = 8.3$	7.06–7.15	7.03 (t) $^{3}J_{H6'} = 8.8$ $^{4}J_{F3'} = 8.8$	7.00 (t) $^{3}J_{H6'} = 8.7$ $^{4}J_{F3'} = 8.7$	6.65 (dd) $^{3}J_{H6'} = 8.6$	7.12 (ddd) $^{3}J_{H6'} = 8.9$ $^{3}J_{F4'} = 10.5$ $^{5}J_{F2'} = 1.8$	–
H6′	7.14 (dd)	7.06–7.15	7.32 (dd) $^{4}J_{H2'} = 1.6$	7.37 (dd) $^{4}J_{H2'} = 1.6$	7.64 (m)	7.26 (ddd) $^{4}J_{F2'} = 7.8$ $^{4}J_{F4} = 5.8$	7.67 (dd) $^{3}J_{F5'} = 11.9$ $^{4}J_{F2'} = 7.9$
H2″/H6″	7.95 (m)	7.95 (m)	7.95 (m)	7.99 (m)	8.01 (m)	8.02 (m)	8.00 (m)
H3″/H5″	7.47 (m)	7.47 (m)	7.48 (m)	7.65–7.53	7.54 (m)	7.55 (m)	7.55 (m)
H4″	7.53 (m)	7.55 (m)	7.58–7.53	7.65–7.53	7.63 (m)	7.65 (m)	7.63 (m)

[a] Published in Ref. [10]

[b] Not observed in ^{19}F NMR

shows that in all cases, tautomer **a** is observed in the crystal.

Concerning the rotamers of compounds **6a** and **12a**, the better correlations are obtained for the OH/F2 one:

$$(0.99 \pm 0.01)\mathbf{6a},\ n = 17,\ R^2 = 0.998 \text{ and} \quad (7)$$

$$(0.996 \pm 0.009)\mathbf{12a},\ n = 15,\ R^2 = 0.999 \quad (8)$$

Compound **5** in the solid state is a mixture of two rotamers **5a** and **5a′** (see Fig. 12 for the ^{13}C CPMAS spectrum). The signals assignment was made using the data in solution (Tables 6, 8) as well as the theoretical calculations (Table 11). In the spectrum of Fig. 12, it should be noted the multiplet appearance of C4 signals, probably due to residual couplings with ^{19}F.

The appearance of the CF_3 group deserves some comments. In Fig. 13, we represent the signal of this group in the case of compound **8**. All other compounds (**9–13**) show similar signals, meaning that in our experimental conditions of ^{19}F{^{1}H} MAS spectra, the trifluoromethyl group appears as a singlet. Other authors have reported spectra in the form of complex multiplets [18], but using different conditions.

Another aspect is that according to the calculations for a not-rotating CF_3 group, the signals of the three fluorine atoms are quite different, for instance CF_3 **8a**. −84.9, −77.3, −72.2 ppm → mean −78.1, $\Delta\delta = 12.7$ ppm; CF_3 **9a**. −85.2, −76.6, −72.7 → mean −78.2, $\Delta\delta = 12.5$ ppm. Since only a signal situated close to the average chemical shift is observed, this signify that the CF_3 group is freely rotating or, at least, oscillating around its equilibrium geometry (libration). However, in compound **9** (two independent molecules, see Fig. 8), the F atoms of the CF_3 groups do not show disorder.

Although there is no disorder in the position of the fluorine atoms (the ADP are rather normal) [19], we have to assume fast 60° oscillations about the C1–CF_3 bond that will exchange both kinds of F atoms. Similar, but less clear examples of a CF_3 group that appears static in crystallography and dynamic in solid-state NMR have been reported [20–23].

To better understand the behavior of the enols of β-diketones in the solid state, we have carried out Quantum ESPRESSO calculations on the three compounds reported in this paper (**5**, **7** and **9**) as well as on compound **3** previously described [10].

Table 5 ^{1}H NMR data of compounds **8–13**

	8[a] $CDCl_3$	**9** $CDCl_3$	**10** $CDCl_3$	**11** $CDCl_3$	**12** $CDCl_3$	**12** 85 % $CDCl_3$ + 15 % DMSO	**13** $CDCl_3$	**13** 85 % $CDCl_3$ + 15 % DMSO
H2	6.01 (s)	6.03 (s)	6.00 (s)	6.01 (s)	6.03 (s)	5.95 (s)	6.01 (s)	5.81 (s)
OH-enol	14.36	14.15	14.21	14.29	14.20	9.60	14.2	10.30
H4	6.43 (d) $^{3}J_{H5} = 15.7$	6.49 (d) $^{3}J_{H5} = 15.8$	6.42 (d) $^{3}J_{H5} = 15.7$	6.57 (d) $^{3}J_{H5} = 15.9$	6.64 (d) $^{3}J_{H5} = 16.0$	6.56 (d) $^{3}J_{H5} = 16.0$	6.52 (d) $^{3}J_{H5} = 15.9$	6.30 (d) $^{3}J_{H5} = 15.9$
H5	7.71 (d)	7.70 (d)	7.66 (dd) $^{5}J_{F3'} = 0.9$[b]	7.81 (d)	7.77 (d)	7.72 (d)	7.75 (dd) $^{5}J_{F5'} = 1.1$	7.53 (dd) $^{5}J_{F5'} = 1.1$
H2′	7.06 (d) $^{4}J_{H6'} = 1.9$	7.16–7.08	7.32 (dd) $^{3}J_{F3'} = 11.2$ $^{4}J_{H6'} = 2.1$	–	–	–	–	–
H3′	3.96 (OMe)	3.94 (OMe)	–	6.64 (dd) $^{3}J_{F2'} = 11.8$ $^{4}J_{H5'} = 2.5$	5.40 (OH)	9.60 (OH)	7.29 (dd) $^{3}J_{F2'} = 10.3$ $^{4}J_{F5'} = 6.4$	6.52 (dd) $^{3}J_{F2'} = 11.6$ $^{4}J_{F5'} = 7.2$
4′-OH	5.95	–	5.49	5.36	–	–	[c]	10.30
H5′	6.96 (d) $^{3}J_{H6'} = 8.3$	7.16–7.08	7.05 (dd) $^{3}J_{H6'} = 8.4$ $^{4}J_{F3'} = 8.8$	6,68 (dd) $^{3}J_{H6'} = 8.5$	6.97 (td) $^{3}J_{H6'} = 9.1$ $^{3}J_{F4'} = 9.1$ $^{5}J_{F2'} = 1.9$	6.82 (ddd) $^{3}J_{F4'} = 9.9$ $^{3}J_{H6'} = 8.8$ $^{5}J_{F2'} = 1.8$	–	–
H6′	7.15 (dd)	7.16–7.08	7.27 (dd)	7.45 (dd) $^{4}J_{F2'} = 8.5$	7.08 (ddd) $^{4}J_{F2'} = 7.5$ $^{4}J_{F4'} = 5.9$	6.92 (ddd) $^{4}J_{F2'} = 7.4$ $^{4}J_{F4'} = 5.7$	6.81 (dd) $^{3}J_{F5'} = 11.0$ $^{4}J_{F2'} = 7.2$	7.05 (dd) $^{3}J_{F5'} = 11.3$ $^{4}J_{F2'} = 6.8$

[a] Published in Ref. [10]

[b] Not observed in ^{19}F NMR

[c] Not observed

Two features are worth mentioning concerning periodic calculations of chemical shifts, using the GIPAW DFT-D method: (1) to start the calculations, the X-ray (or neutron diffraction) structure must be known; (2) contrary to solution NMR, there are almost no empirical equations to transform the calculated [24, 25] absolute shieldings (σ, ppm) into chemical shifts (δ, ppm), although one of us (M.B.F.) has already published an equation to do this for ^{13}C data [26]:

$$\delta(\text{ppm}) = (163 \pm 2) - (0.897 \pm 0.02)\sigma(\text{ppm}), \quad R^2 = 0.9805 \tag{9}$$

The calculations for the crystal structures employing pbe-rrjkus-gipaw-dc are named as PBE-crystal. As it is indicated in the Computational details section, all the systems have been optimized with QE at the same level of theory, pbe-rrjkus-gipaw-dc. We have calculated four ketoenols: The three we have determined their X-ray structures in this paper and one from a previous publication **8** [10]; they are represented in Fig. 14 as the tautomer observed by crystallography. The results are reported in Table 12.

In the case of compounds **5**, **7** and **8**, a set of four identical molecules have been used; thus, the PBE-crystal calculations are identical for the four molecules. In the case of compound **9**, four different molecules have been calculated (total, eight molecules, four pairs of identical molecules, Fig. 15).

A statistical analysis of the data of Table 12 leads to the following equations where dummy variables corresponding to the ^{13}C and ^{19}F signals of the CF_3 have been introduced to account for a systematic deviation of the atoms of this substituent in the solid state [27].

$$^{13}\text{C CPMAS} = -(2.0 \pm 2.1) + (1.01 \pm 0.02)\ \text{Calc. } \delta\text{DMSO} - (5.3 \pm 3.8)^{13}CF_3, \quad n = 77,\ R^2 = 0.982 \tag{10}$$

Table 6 ^{13}C NMR data of compounds **2–7** (chemical shifts in ppm, SSCC in Hz; when not specified they are J_{CH})

	2 [8, 10]		**3** [10]		**4** [10]		**5**		**6**		**7**	
	$CDCl_3$	CPMAS	$CDCl_3$	CPMAS	DMSO-d_6	CPMAS	DMSO-d_6	CPMAS	DMSO-d_6	CPMAS	DMSO-d_6	CPMAS
C1	188.4	187.2	189.3[a]	187.1	187.5[a]	191.6	188.0[a]	192.8	189.1[a] $^2J = {}^3J = {}^3J = 3.8$	193.8	188.5[a] $^2J = {}^3J = {}^3J = 3.9$	194.9
C2	97.2 $^1J = 163.4$	97.8	97.6 $^1J = 163.7$	98.1	97.1 $^1J = 166.0$	97.4	97.5 $^1J = 166.3$ $^3J = 2.3$	98.1	98.1 $^1J = 166.9$ $^3J = 2.0$	103.0	97.7 $^1J = 166.2$ $^3J = 2.4$	100.4
C3	180.5 $^2J_{H2,H4,OH} = {}^3J_{H5} = 4.4$	180.2	179.2[b]	180.7	180.6[b]	176.2	180.1[b] $^3J = 3.5$ $^2J = {}^2J = 6.0$	177.0	178.6[b] $^3J = 4.0$ $^2J = {}^2J = 6.3$	174.9	179.9[b] $^3J = 3.8$ $^2J = {}^2J = 6.1$	174.8
C4	121.0 $^1J = 156.9$	119.8	123.2 $^6J_{F4'} = 1.3$ $^1J = 157.4$	123.5	121.6 $^1J = 159.8$	119.7	122.2 $^1J = 161.2$ $^2J = {}^3J = 4.1$ $^4J_{F2'} = 6.2$	122.5/117.4	125.5 $^1J = 161.6$ $^4J_{F2'} = 6.3$ $^6J_{F4'} = 2.4$	124.2	123.6 $^1J = 161.3$ $^4J_{F2'} = 5.7$	121.2
C5	140.4 $^1J = 155.2$ $^3J = {}^3J = 4.4$	142.4	139.0 $^5J_{F4'} = 1.2$ $^1J = 156.8$	138.7	139.3 $^1J = 154.2$	139.8	132.3 $^1J = 156.7$ $^3J_{F2'} = 2.5$	135.8	131.2 $^1J = 159.7$ $^3J_{F2'} = {}^5J_{F4'} = 2.3$	134.3	131.0 $^1J = 157.9$ $^3J_{F2'} = {}^4J_{F5'} = 1.9$	129.3
C1′	127.7	127.8	131.7 $^4J_{F4'} = 3.9$	131.3	126.6 $^3J_{F3'} = 6.8$	129.9	113.4 $^2J_{F2'} = 11.5$	113.6	119.5 $^2J_{F2} = 6.8$ $^4J_{F4'} = 2.4$	119.6	113.1 $^2J_{F2'} = 14.0$ $^3J_{F5'} = 6.7$	114.4
C2′	109.6 $^1J = 156.6$ $^3J = {}^3J = 6.5$	105.8	112.4 $^3J_{F4'} = 1.9$ $^1J = 158.3$ $^3J = {}^3J = 6.0$	114.8	115.4 $^2J_{F3'} = 18.7$ $^1J = 160.9$	112.3	161.9 $^1J_{F2'} = 251.4$ $^3J = 11$ $^3J = {}^2J = 5$	164.5/160.4[c]	151.2[e] $^1J_{F2'} = 249.1$ $^3J_{F4'} = 6.5$	151.9 (br)	157.1 $^1J_{F2'} = 248.3$ $^4J_{F5'} = 1.5$	158.1 155.4
C3′	146.9	147.0	148.0 $^2J_F = 11.4$	148.5	151.1 $^1J_{F3'} = 242.2$	152.2 149.5	103.0 $^2J_{F2'} = 23.8$ $^1J = 162.7$ $^3J = 5.2$	104.6[d]	134.2 $^2J_{F2'} = {}^2J_{F4'} = 16.1$ $^3J = 7.0$	134.3	105.1 $^2J_{F2'} = 26.6$ $^3J_{F5'} = 3.3$ $^1J = 164.4$	106.9
C4′	147.8	149.8	153.5 $^1J_{F4'} = 251.4$ $^3J = {}^3J = 8.6$ $^2J = 3.2$	153.1	147.12 $^2J_{F3'} = 12.4$	146.2	161.3 $^3J_{F2'} = 12.6$ $^2J = 12.0$	161.6/159.9	152.3[d] $^1J_{F4'} = 246.6$ $^3J_{F2'} = 6.2$	151.9 (br)	148.3 $^2J_{F5'} = 14.6$ $^3J_{F2'} = 12.6$	147.3
C5′	114.9 $^1J = 163.2$	115.8	116.5 $^2J_{F4'} = 18.7$ $^1J = 163.4$	116.4	118.0 $^3J_{F3'} = 2.6$ $^1J = 159.8$	118.6	112.7 $^4J_{F2'} = 2.5$ $^1J = 162.6$ $^3J = 5.1$	113.6[d]	112.2 $^2J_{F4'} = 19.2$ $^4J_{F2'} = 3.7$ $^1J = 166.8$	112.3	148.0 $^1J_{F5'} = 238.7$ $^4J_{F2'} = 2.2$	149.7 147.3
C6′	122.9 $^1J = 160.9$ $^3J = {}^3J = 6.2$	126.5	121.3 $^3J_{F4'} = 7.4$ $^3J = {}^3J = 6.3$ $^1J = 162.8$	119.5	125.7 $^4J_{F3'} = 2.1$ $^1J = 163.8$	127.9	130.3 $^3J_{F2'} = 5.1$ $^1J = 161.1$ $^2J = {}^3J = 5.2$	128.4[c]	117.9 $^3J_{F4'} = 8.8$ $^3J_{F2'} = 3.3$ $^1J = 167.7$	112.3	116.0 $^2J_{F5'} = 21.0$ $^3J_{F2'} = 5.0$ $^1J = 163.3$	111.4

Table 6 continued

	2 [8, 10]		**3** [10]		**4** [10]		**5**		**6**		**7**	
	$CDCl_3$	CPMAS	$CDCl_3$	CPMAS	DMSO-d_6	CPMAS	DMSO-d_6	CPMAS	DMSO-d_6	CPMAS	DMSO-d_6	CPMAS
C1″	136.3 $^3J = {}^3J = 7.3$	136.2	136.2 $^3J = {}^3J = 7.2$	137.2	135.4 $^3J = {}^3J = 7.0$	136.2	135.4 $^3J = {}^3J = 7.3$	135.8	135.4 $^3J = {}^3J = 7.3$	136.2	135.4 $^3J = {}^3J = 7.3$	134.4
C2″/C6″	127.3 $^1J = 160.4$ $^3J = {}^3J = 6.6$	126.5	127.3 $^1J = 160.8$ $^3J = {}^3J = 6.7$	127.5	127.1 $^1J = 161.2$ $^3J = {}^3J = 6.5$	127.9	127.2 $^1J = 162.2$ $^3J = {}^3J = 6.7$	128.4	127.4 $^1J = 161.9$ $^3J = {}^3J = 6.5$	128.6	127.2 $^1J = 161.5$ $^3J = {}^3J = 6.5$	126.2 127.6
C3″/C5″	128.6 $^1J = 161.4$ $^3J = 7.5$	126.5	128.6 $^1J = 161.5$ $^3J = 7.6$	128.4	128.8 $^1J = 162.3$ $^3J = 7.5$	128.8	128.9 $^1J = 161.8$ $^3J = 7.6$	128.4	128.9 $^1J = 162.4$ $^3J = 7.5$	128.6	128.9 $^1J = 162.3$ $^3J = 7.4$	129.3
C4″	132.4 $^1J = 161.0$ $^3J = {}^3J = 7.6$	132.1	132.6 $^1J = 161.5$ $^3J = {}^3J = 7.6$	130.0	132.8 $^1J = 161.8$ $^3J = {}^3J = 7.3$	133.9	132.9 $^1J = 162.0$ $^3J = {}^3J = 7.8$	134.0	133.8 $^1J = 162.5$ $^3J = {}^3J = 7.3$	134.3	133.0 $^1J = 161.9$ $^3J = {}^3J = 7.3$	132.9

[a] It shows HMBC correlation with Ho and H2

[b] It shows HMBC correlation with H4 y H2, and in some cases also with H5

[c] Actually C–F at positions 2′ and 6′

[d] Non-standard numbering for positions 3′ and 5′

[e] To assign C2′ in compound **6**, we have used the HMBC correlation with H5 that it is absent in C4′ as well as the $^1J_{C2F2} > {}^1J_{C4F4}$ coupling constant values

Other signals: OCH_3: **2**: 56.0, $^1J = 145.1$ ($CDCl_3$), 56.2 (CPMAS); **3**: 56.2, $^1J = 144.9$ ($CDCl_3$); 54.5 (CPMAS)

Table 7 ^{13}C NMR data of compounds **8–13** (chemical shifts in ppm, SSCC in Hz; when not specified they are J_{CH})

	8 [10]		**9**		**10**		**11**		**12**		**13**	
	$CDCl_3$	CPMAS	$CDCl_3$	CPMAS	$CDCl_3$	CPMAS	$CDCl_3$	CPMAS	$CDCl_3$ + DMSO	CPMAS	$CDCl_3$ + DMSO	CPMAS
CF_3	116.9 $^1J_F = 285.2$	115.6	116.7 $^1J_F = 286.0$	117.3 (br)	116.7 $^1J_F = 286.5$	116.5 (vbr)	116.3 $^1J_F = 285.2$	115.8 (br)	116.4 $^1J_F = 285.5$	120.0	115.9 $^1J_F = 286.5$	117.8
C1	179.5 $^2J_F = 35.9$ $^2J = 2.7$	178.2	180.4 $^2J_F = 35.8$	180.1	180.2 $^2J_F = 36.1$ $^2J = 2.6$	179.3	179.7 $^2J_F = 36.2$	181.2	180.2 $^2J_F = 35.8$	183.0	178.8 $^2J_F = 34.3$	160.5
C2	95.1 $^1J = 165.8$	94.8	95.6 $^3J_F = 1.7$	95.2	95.5 $^3J_F = 1.6$ $^1J = 168.9$	95.1	95.1 $^1J = 169.0$	95.3	95.6 $^1J = 168.8$	96.6	94.7	96.3
C3	181.9 $^2J = {}^2J = {}^3J = 5.1$	181.6	180.8	181.4	181.0 $^2J = {}^2J = 6.3$ $^3J = 3.9$	180.1	181.0	182.2	180.5	183.0	180.4	181.9
C4	118.5 $^1J = 158.6$	115.6	120.8 $^6J_{F4'} = 2.5$	118.0	120.0 $^1J = 159.7$ $^3J = {}^2J = 2.6$	117.7	120.6 $^4J_{F2'} = 7.3$ $^1J = 163.5$	116.3	122.4 $^4J_{F2'} = 7.7$ $^1J = 162.6$	125.0	119.8	118.6
C5	144.1 $^1J = 155.6$ $^3J = {}^3J = 4.2$	142.5	142.6 $^5J_{F4'} = 1.9$	143.2/146.3	142.3 $^4J_{F3'} = 2.7$ $^1J = 156.8$	142.7	136.0 $^1J = 160.3$	136.2	135.9 $^1J = 159.0$	143.6	134.8	135.3
C1′	126.8	126.4	130.9 $^4J_{F4'} = 4.3$	130.9/132.1	127.7 $^3J_{F3'} = 6.4$	124.9	115.0 $^2J_{F2'} = 11.2$	112.3	118.9 $^2J_{F2'} = 9.2$ $^4J_{F4'} = 2.6$	118.5	112.2	112.8
C2′	109.8 $^1J = 162.3$ $^3J = {}^3J = 6.6$	106.4	112.7 $^3J_{F4'} = 3.1$	114.1	114.9 $^2J_{F3'} = 18.7$ $^1J = 161.4$ $^3J = 6.5$ $^3J = 8.6$	110.4	162.36 $^1J_{F2'} = 256.2$	161.2 (br)	151.8 $^1J_{F2'} = 251.5$ $^3J_{F4'} = 6.3$	153.1 151.0	157.4 $^1J_{F2'} = 251.0$	157.9
C3′	147.0	149.1	148.3 $^2J_{F4'} = 11.4$	146.9	151.1 $^1J_{F3'} = 239.3$	150.5 (br)	103.5 $^2J_{F2'} = 25.2$ $^1J = 163.0$ $^3J = 4.8$	101.3	134.7 $^2J_{F2'} = {}^2J_{F4'} = 16.0$	132.6	104.7 $^2J_{F2'} = 27.1$ $^3J_{F5'} = 2.6$	103.5
R_3	56.0 $^1J = 145.2$	54.8	56.3	55.7/54.6	–	–	–	–	–	–	–	–
C4′	149.0	150.6	154.3 $^1J_{F4'} = 253.5$	151.7/154.0	146.2 $^2J_{F3'} = 14.6$	148.3	158.9 $^3J_{F2'} = 13.4$	163.3	154.1 $^1J_{F4'} = 249.6$ $^3J_{F2'} = 6.3$	155.0 153.1	148.8 $^2J_{F5'} = {}^3J_{F2'} = 12.5$	151.1
C5′	115.1 $^1J = 163.3$	115.6	116.8 $^2J_{F4'} = 19.2$	116.0/118.0		115.0	111.9 $^4J_{F2'} = 2.4$ $^1J = 162.6$	111.3	111.8 $^2J_{F4'} = 19.5$ $^4J_{F2'} = 3.1$ $^1J = 165.9$	111.9	147.5 $^1J_{F5'} = 240.0$ $^4J_{F2'} = 2.5$	147.3

Table 7 continued

	8 [10]		**9**		**10**		**11**		**12**		**13**	
	$CDCl_3$	CPMAS	$CDCl_3$	CPMAS	$CDCl_3$	CPMAS	$CDCl_3$	CPMAS	$CDCl_3$ + DMSO	CPMAS	$CDCl_3$ + DMSO	CPMAS
C6′	124.0	126.4	122.2	118.0	126.3	130.8	130.5	126.9	118.1	120.9	114.0	110.8
	$^1J = 162.3$		$^3J_{F4'} = 6.9$		$^4J_{F3'} = 3.0$		$^3J_{F2'} = 4.8$		$^3J_{F4'} = 8.6$		$^2J_{F5'} = 20.7$	
					$^1J = 156.8$		$^1J = 162.8$		$^1J = 163.3$		$^3J_{F2'} = 4.9$	
							$^3J = 4.8$					

$$^{13}\text{C CPMAS} = (161.0 \pm 0.6) - (0.96 \pm 0.02)\ \text{Calc.}\sigma\text{PBE} - \text{crystal} - (9.4 \pm 4.0)\,^{13}CF_3, \quad n = 77,\ R^2 = 0.980 \tag{11}$$

$$^{19}\text{F MAS} = -(6.3 \pm 13.4) + (0.92 \pm 0.12)\ \text{Calc.}\delta\text{DMSO}, \quad n = 7,\ R^2 = 0.921 \tag{12}$$

$$^{19}\text{F MAS} = (154.3 \pm 23.4) - (1.02 \pm 0.09)\ \text{Calc.}\sigma\text{PBE} - \text{crystal}, \quad n = 7,\ R^2 = 0.962 \tag{13}$$

$$^{19}\text{F MAS} = (93.2 \pm 21.0) - (0.80 \pm 0.08)\ \text{Calc.}\sigma\text{PBE} - \text{crystal} + (14.1 \pm 3.9)\ C^{19}F_3, \quad n = 7,\ R^2 = 0.991 \tag{14}$$

$$^{13}\text{C \&}\,^{19}\text{F only for } \mathbf{5a} + \mathbf{5a'}:\ \text{Calc.}\sigma\text{CASTEP/PBE} = (7.0 \pm 0.4) + (0.961 \pm 0.007)\ \text{Calc.}\sigma\text{PBE} - \text{crystal}, \quad n = 36,\ R^2 = 0.998 \text{ (for CASTEP, see below)} \tag{15}$$

$$^{13}\text{C only for } \mathbf{5a} + \mathbf{5a'}:\ \text{CPMAS} = -(161.0 \pm 1.0) - (0.98 \pm 0.03)\ \text{Calc.}\sigma\text{PBE} - \text{crystal}, \quad n = 34,\ R^2 = 0.978 \tag{16}$$

$$^{13}\text{C only for } \mathbf{5a} + \mathbf{5a'}:\ \text{CPMAS} = -(167.4 \pm 0.9) - (1.00 \pm 0.03)\ \text{Calc.}\sigma\text{CASTEP/PBE}, \quad n = 34,\ R^2 = 0.985 \tag{17}$$

For solid-state ^{13}C CPMAS results, Eqs. 10 and 11 are rather similar, but Eq. 10 is more intuitive because its intercept is 0 and its slope 1.0. On the other hand, for solid-state ^{19}F MAS results, Eq. 13 is better than Eq. 12; the addition of a dummy variable for correcting the CF_3 anomaly results in a large improvement and a coefficient of −14.1 ppm (Eq. 10).

In the case of compound **5**, we have carried out CASTEP calculations besides PBE ones (Table 12). The absolute shieldings calculated by both methods are highly correlated (Eq. 15), but CASTEP seems a little better (compare Eqs. 16 and 17). However, since CASTEP calculations have been used for the assignment of Fig. 12, this could explain the slight improvement. The intercepts of Eqs. 11 and 16 (161.0 ppm) are similar to that of Eq. 9 (163 ppm) and correspond roughly (exactly if the slope = 1) to the absolute shielding of TMS in the solid state calculated with the same method.

Table 8 ^{19}F NMR data of compounds **3–7** (chemical shifts in ppm, SSCC in Hz)

	3[a]			**4**[a]			**5**		**6**		**7**	
	$CDCl_3$	DMSO-d_6	MAS	$CDCl_3$	DMSO-d_6	MAS	DMSO-d_6	MAS[b]	DMSO-d_6	MAS	DMSO-d_6	MAS
F2′	–	–	–	–	–	–	−113.5 $^3J_{H3'} = 12.8$ $^4J_{H6'} = 9.2$[c]	−103.2 (74 %) −107.3 (26 %)	−134.1 $^3J_{FF} = 14.5$ $^4J_{H6'} = 7.8$ $^5J_{H5'} = 1.8$	−129.4	−118.6 $^5J_{FF} = 15.0$ $^3J_{H3'} = 12.8$ $^4J_{H6'} = 7.9$	−115.4
F3′	–	–	–	−140.6 $^3J_{H2'} = 11.3$[c] $^4J_{H5'} = 8.8$	−135.7 $^3J_{H2'} = 12.0$[c] $^4J_{H5'} = 8.7$	−126.3	–	–	–	–	–	–
F4′	−132.0 $^3J_{H5'} = {}^4J_{H2'} = 9.3$[c] $^4J_{H6'} = 5.2$[c]	−131.8 $^3J_{H5'} = {}^4J_{H2'} = {}^4J_{H6'} = 8.3$[c]	−126.1	–	–	–	–	–	−128.2 $^3J_{FF} = 14.5$ $^4J_{H5'} = 10.5$ $^5J_{H6'} = 5.8$	−129.4	–	–
F5′	–	–	–	–	–	–	–	–	–	–	−140.1 $^5J_{FF} = 15.0$ $^3J_{H6'} = 11.9$ $^4J_{H3'} = 7.4$	−138.2

[a] Reported in Ref. [10] except the solid NMR spectra

[b] Remember that the F atom is disordered into two position, 2′ (70 %) and 6′ (30 %) (see crystallographic part, Fig. 6)

[c] The SSCC have been measured only in the ^{19}F NMR spectra

Table 9 ^{19}F NMR data of compounds **8–13** (chemical shifts in ppm, SSCC in Hz)

	8[a]				**9**		**10**		**11**		**12**		**13**	
	$CDCl_3$	DMSO-d_6	HMPA-d_{18}	MAS	$CDCl_3$	MAS	$CDCl_3$	MAS	$CDCl_3$	MAS	$CDCl_3$ + DMSO-d_6	MAS	$CDCl_3$ + DMSO-d_6	MAS
CF_3	−77.5	−75.8 (+) −76.6 (−)	−76.8 (−) −77.7 (+)	−74.1	−77.6	−74.1	−77.6	−72.1	−77.6	−73.4	−77.6	−73.8	−77.6	−74.2
F2′	–	–	–	–	–	–	–	–	−111.0 $^3J_{H3'} = 11.8$ $^4J_{H6'} = 8.5$	−113.9	−133.5 $^3J_{FF} = 16.4$ $^4J_{H6'} = 7.4$ $^5J_{H5'} = 1.8$	−126.7	−117.7 $^5J_{FF} = 14.3$ $^3J_{H3'} = 11.6$ $^4J_{H6'} = 6.8$	−119.1
F3′	–	–	–	–	–	–	−140.1 $^3J_{H2'} = 11.2$ $^4J_{H5'} = 8.8$	−134.0	–	–	–	–	–	–
F4′	–	–	–	–	−129.8 $^3J_{H5'} = 9.1$[b] $^4J_{H2'} = 8.0$[b] $^4J_{H6'} = 5.7$[b]	−129.3 −130.6	–	–	–	–	−127.5 $^3J_{FF} = 16.4$ $^3J_{H5'} = 9.9$ $^4J_{H6'} = 5.7$	−130.2	–	–
F5′	–	–	–	–	–	–	–	–	–	–	–	–	−141.2 $^5J_{FF} = 14.3$ $^3J_{H6'} = 11.3$ $^4J_{H3'} = 7.2$ $^5J_{H5} = 1.1$	−138.4

[a] Reported in Ref. [10] except the solid NMR spectra

[b] The SSCC have been measured only in the ^{19}F NMR spectra

Table 10 Population of **a** and **b** tautomers, equilibrium constants K, differences in free energy ΔG (kJ mol^{-1}) obtained from experimental and calculated chemical shifts

Comp.	R	Solv.	Tautomer **a**	Tautomer **b**	K (**b**/**a**)	ΔG (298.15 K) (kJ mol^{-1})	E_{rel} (kJ mol^{-1}) **b**–**a**	X-ray
2	C_6H_5	$CDCl_3$	0.74	0.26	0.351	2.6	3.8	**a**
3	C_6H_5	$CDCl_3$	0.78	0.22	0.282	3.1	3.9	**a**
4	C_6H_5	DMSO-d_6	0.68	0.32	0.471	1.9	3.9	**a**
5	C_6H_5	DMSO-d_6	0.84	0.16	0.190	4.1	4.0	**a**
6	C_6H_5	DMSO-d_6	0.82	0.18	0.220	3.8[a]	4.0[b]	
7	C_6H_5	DMSO-d_6	0.83	0.17	0.205	3.9	3.9	**a**
8[c]	CF_3	$CDCl_3$	0.82	0.18	0.220	3.8	8.8	**a**
9	CF_3	$CDCl_3$	0.85	0.15	0.176	4.3	8.5	**a**
10	CF_3	$CDCl_3$	0.82	0.17	0.207	3.9	8.5	
11	CF_3	$CDCl_3$	0.86	0.13	0.151	4.7	8.6	
12	CF_3	DMSO-d_6	0.81	0.19	0.235	3.6[a]	8.3[b]	
13	CF_3	DMSO-d_6	0.85	0.14	0.165	4.5	8.2	
14	CH_3	$CDCl_3$	0.83	0.18	0.217	3.8	1.7	**a**
15	CH_3	$CDCl_3$	0.84	0.17	0.202	4.0	3.9	
16	C_6H_5	$CDCl_3$	0.75	0.24	0.320	2.8	4.0	
17	C_6H_5	$CDCl_3$	0.53	0.47	0.887	0.3	2.0	

[a] Values corresponding to the OH/F2′ rotamer

[b] Mean values of both OH rotamers

[c] In DMSO-d_6 by direct integration in ^{19}F NMR 85 % **a**–15 % **b** [10]

Concerning the splittings, we note the following facts:

- Compound **5**, one independent molecule but splitting observed on C2′ and F2′, i.e., on the atoms of the CF bond: This is related to the positional disorder determined by crystallography (see Fig. 6). According to crystallography, there is 70 % of s*E* conformation (F6) and 30 % of s*Z* conformation (F6′, the single *E*/single *Z* nomenclature based on the substituents about the C1–C7 bond, X-ray, or C1′–C5, NMR): This is in perfect agreement with the ^{19}F MAS results (Table 8), within experimental errors (Fig. 16). In ^{13}C CPMAS, the integration is not possible due to the proximity of the signals which include that of C4′ (Fig. 12), but in any case there is a signal two or three times more intense than the other.
- Compound **7**, one independent molecule but splitting observed on C2′, C5′ and C2″. The two first correspond to CF bonds, and the last one to the difference between C2″ and C6″ *ortho* carbons.
- Compound **8**, one independent molecule and no splitting observed.

In the case of compound **9**, the absolute shieldings of four different molecules have been calculated (Table S2 of Supplementary Material). Using Eqs. 11 and 15, we have calculated the corresponding chemical shifts (Table 12). This allows to assign some splittings in the ^{13}C CPMAS NMR (Figs. 17, 18).

The result is not entirely satisfying because the experimental splitting (between 0.6 and 2.3 ppm) does not correspond to the calculated maximum differences (between 0.18 and 2.92 ppm).

Experimental section

Materials

All chemicals cited in the synthetic procedures are commercial compounds. Melting points were determined by DSC with a SEIKO DSC 220 C connected to a model SSC5200H disk station. Thermograms (sample size 0.003–0.005 g) were recorded with a scan rate of 5.0 °C. Column chromatography was performed on silica gel (Merck 60, 70–230 mesh) and elemental analyses using a PerkinElmer 240 apparatus.

Synthesis

(*E*)-5-(4-hydroxy-3-methoxyphenyl)-1-phenylpent-4-ene-1,3-dione [**2**, m.p. 159.9 °C] [9], (*E*)-5-(4-fluoro-3-methoxyphenyl)-1-phenylpent-4-ene-1,3-dione [**3**, m.p. 127.2 °C]

Table 11 Experimental solution and solid state together with calculated (GIAO) in DMSO solution and in the solid state (QE)

	DMSO-d_6 **5**	[CP]MAS	Calc. δ DMSO **5a**	Calc. σ PBE-crystal **5a**	Calc. σ CASTEP **5a**
C1	188.0	192.8	187.7	−25.52	−18.29
C2	97.5	98.1	95.3	63.55	69.38
C3	180.1	177.0	173.7	−15.63	−9.08
C4	122.2	122.5	125.2	39.42	45.76
C5	132.3	135.8	133.8	23.33	29.02
C1′	113.4	113.6	117.5	46.48	54.03
C2′	161.9	160.4	165.5	−8.63	−2.04
C3′	103.0	104.6	101.5	57.57	64.31
C4′	161.3	159.9	158.5	−2.03	4.75
C5′	112.7	113.6	111.1	48.28	53.66
C6′	130.3	128.4	136.6	24.96	30.86
C1″	135.4	135.8	137.5	25.34	32.96
C2″	127.2	128.4	128.0	33.59	39.85
C3″	128.9	128.4	127.8	32.36	38.85
C4″	132.9	134.0	131.7	27.99	33.54
C5″	128.9	128.4	127.8	31.10	37.34
C6″	127.2	128.4	128.0	33.88	40.23
F2′	−113.5	−103.2 (74 %)	−106.4	246.21	241.97
	5		**5a′**	**5a′**	**5a′**
C1	188.0	192.8	187.9	−25.42	−18.9
C2	97.5	98.1	94.9	64.16	69.01
C3	180.1	177.0	173.5	−14.74	−8.14
C4	122.2	117.4	119.2	46.19	52.01
C5	132.3	135.8	129.2	28.58	33.79
C1′	113.4	113.6	117.2	47.44	54.3
C2′	161.9	164.5	165.6	−7.63	−1.44
C3′	103.0	104.5	102.6	50.12	63.73
C4′	161.3	164.5	159.6	−4.45	1.6
C5′	112.7	113.6	109.1	58.45	55.87
C6′	130.3	128.4	126.1	35.82	40.55
C1″	135.4	135.8	137.8	25.18	31.97
C2″	127.2	128.4	128.0	33.52	39.2
C3″	128.9	128.4	127.8	33.58	39.58
C4″	132.9	134.0	131.8	29.12	34.46
C5″	128.9	128.4	127.8	33.64	36.79
C6″	127.2	128.4	128.8	33.47	39.39
F2′	−113.5	−107.3 (26 %)	−111.8	254.22	250.47
	7		**7a**	**7a**	–
C1	188.5	194.9	190.2	−26.22	
C2	97.7	100.4	97.2	64.26	
C3	179.9	174.8	174.3	−15.07	
C4	123.6	121.2	124.1	42.78	
C5	131.0	129.3	135.7	30.37	
C1′	113.1	114.4	116.6	46.59	
C2′	157.1	156.8[a]	162.5	−3.32	
C3′	105.1	106.9	105.6	57.14	

Table 11 continued

	7		**7a**	**7a**	–
C4′	148.3	147.3	147.8	8.53	
C5′	148.0	148.5[a]	149.2	8.21	
C6′	116.0	111.4	116.6	50.83	
C1″	135.4	134.4	137.3	25.17	
C2″	127.2	127.6	128.5	33.06	
C3″	128.9	129.3	128.7	33.35	
C4″	133.0	132.9	133.8	28.15	
C5″	128.9	129.3	129.1	30.59	
C6″	127.2	126.2	127.9	33.15	
F2′	−118.6	−115.4	−111.6	262.73	
F5′	−140.1	−138.2	−153.8	292.84	
	$CDCl_3$ **8**	[CP]MAS	Calc. δ DMSO-d_6 **8a**	Calc. σ PBE-crystal **8a**	–
$^{13}C\ CF_3$	116.9	115.6	121.6	37.08	
C1	179.5	178.2	179.3	−18.95	
C2	95.1	94.8	95.0	70.01	
C3	181.9	181.6	179.4	−13.40	
C4	118.5	115.6	114.3	47.47	
C5	144.1	142.5	149.4	22.25	
C1′	126.8	126.4	126.9	36.69	
C2′	109.8	106.4	105.8	64.23	
C3′	147.0	149.1	147.2	17.30	
C4′	149.0	150.6	152.5	15.17	
C5′	115.1	115.6	114.2	54.30	
C6′	124.0	126.4	131.2	36.46	
OCH_3	56.0	54.8	54.7	115.64	
$^{19}F\ CF_3$	−77.5	−74.1	−78.1	229.96	
	9		**9a**	**9a**	–
$^{13}C\ CF_3$	116.7	117.3	121.3	33.10	
C1	180.4	180.1	180.7	−18.91	
C2	95.6	95.2	95.9	65.50	
C3	180.8	181.4	179.1	−16.84	
C4	120.8	118.0	118.5	44.11	
C5	142.6	144.8[a]	147.4	15.73	
C1′	130.9	131.5[a]	132.0	30.64	
C2′	112.7	114.1	122.2	45.94	
C3′	148.3	146.9	149.9	12.85	
C4′	154.3	152.9[a]	162.6	2.50	
C5′	116.8	117.0	118.0	47.52	
C6′	122.2	118.0	132.7	45.23	
OCH_3	56.3	55.2[a]	61.0	110.11	
$^{19}F\ CF_3$	−77.6	−74.1	−78.2	225.42	
F4	−129.8	−130.0[a]	−122.3	274.73	

To compare **5a** and **5a′**, we have numbered both isomers in the same manner concerning atoms C1′ to C6′, i.e., C2′ is always the carbon bearing a fluorine atom

[a] Mean values of two signals (see Tables 6, 8 and 9)

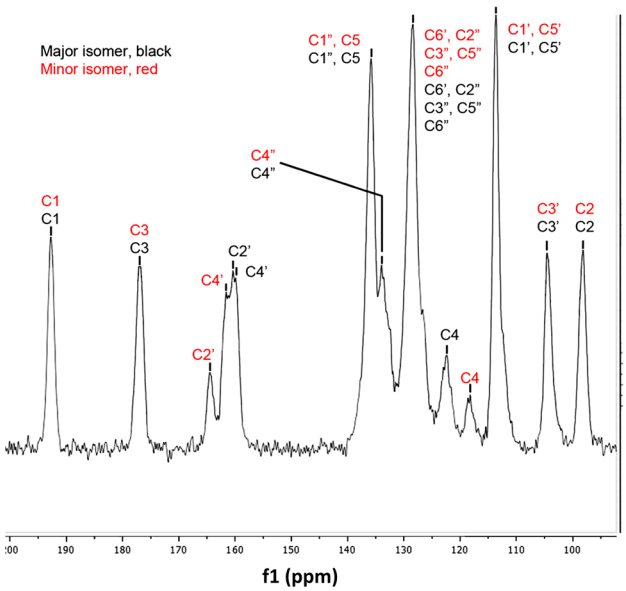

Fig. 12 ^{13}C CPMAS spectrum of (2*Z*,4*E*)-5-(2-fluoro-4-hydroxyphenyl)-3-hydroxy-1-phenylpenta-2,4-dien-1-one (**5a**)

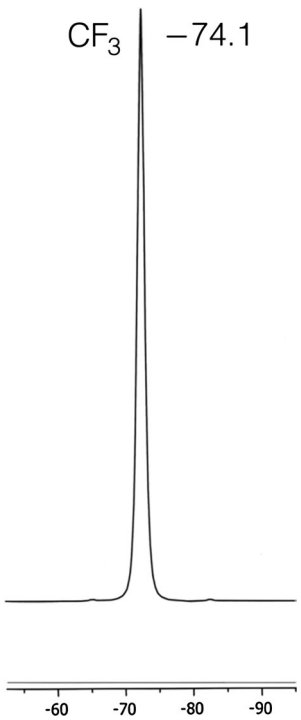

Fig. 13 ^{19}F MAS spectrum of (3*Z*,5*E*)-1,1,1-trifluoro-4-hydroxy-6-(4-hydroxy-3-methoxyphenyl) hexa-3,5-dien-2-one (**8**)

[10], (*E*)-5-(3-fluoro-4-hydroxyphenyl)-1-phenylpent-4-ene-1,3-dione [**4**, m.p. 193.3 °C] [10], (*E*)-1,1,1-trifluoro-6-(4-hydroxy-3-methoxyphenyl)hex-5-ene-2,4-dione [**8**, m.p. 108.9 °C] [10], (*E*)-6-(4-hydroxy-3-methoxyphenyl)hex-5-ene-2,4-dione [**14**, m.p. 141–143 °C] [8], (*E*)-6-(4-hydroxy-3-methoxyphenyl)-3-methylhex-5-ene-2,4-dione [**15**, m.p. 138–140 °C] [8], (*E*)-5-(3,4-dimethoxyphenyl)-1-phenylpent-4-ene-1,3-dione [**16**, m.p. 114–115 °C] [8] and (*E*)-5-(3,4-dimethoxyphenyl)-2-methyl-1-phenylpent-4-ene-1,3-dione [**17**, m.p. 112–113 °C] [8] were prepared as described in the literature.

*(2Z,4E)-5-(2-fluoro-4-hydroxyphenyl)-3-hydroxy-1-phenylpenta-2,4-dien-1-one (**5**)*

1-Phenylbutane-1,3-dione (15 mmol) and boric anhydride (10.5 mmol) were mixed in dry ethyl acetate (11.25 mL) at 50 °C for 30 min. After that, a mixture of 2-fluoro-4-hydroxybenzaldehyde (15 mmol) and tributyl borate (22.5 mmol) in dry ethyl acetate (7.5 mL) was added, with stirring for 30 min at 50 °C. A solution of butylamine (15 mmol) in dry ethyl acetate (7.5 mL) was added slowly over 15 min. The reaction mixture was stirred at 50 °C for 90 min and then overnight at room temperature. Hydrochloric acid (1 M, 30 mL) was then added to the solution at 50 °C, and then, the system was stirred for 1 h. After cooling, the organic layer was separated from the aqueous layer and extracted with 3 × 15 mL of ethyl acetate. The organic layer was washed with water (10 mL, 2 times) and dried (Na_2SO_4), and the solvent was evaporated under vacuum. The crude product was purified by column chromatography with dichloromethane/ethanol (95:5) as eluent, m.p. 164.5 °C (ethanol/dichloromethane) (2.39 g, yield 56 %). $C_{17}H_{13}FO_3$ (284.28): calcd. C 71.82, H 4.61; found C 71.69, H 4.62.

*(2Z,4E)-5-(2,4-difluoro-3-hydroxyphenyl)-3-hydroxy-1-phenylpenta-2,4-dien-1-one (**6**)*

1-Phenylbutane-1,3-dione (15 mmol) and boric anhydride (10.5 mmol) were mixed in dry ethyl acetate (11.25 mL) at 50 °C for 30 min. After that, a mixture of 2,4-difluoro-3-hydroxybenzaldehyde (15 mmol) and tributyl borate (22.5 mmol) in dry ethyl acetate (7.5 mL) was added, with stirring for 30 min at 50 °C. A solution of butylamine (15 mmol) in dry ethyl acetate (7.5 mL) was added slowly over 15 min. The reaction mixture was stirred at 50 °C for 90 min and then overnight at room temperature. Hydrochloric acid (1 M, 30 mL) was then added to the solution at 50 °C, and the system was stirred for 1 h. After cooling, the organic layer was separated from the aqueous layer and extracted with 3 × 15 mL of ethyl acetate. The organic layer was washed with water (10 mL, 2 times) and dried (Na_2SO_4), and the solvent was evaporated under vacuum. The crude product was purified by column chromatography with dichloromethane as eluent, m.p. 195.0 °C (ethanol/dichloromethane) (1.64 g, yield 36 %).

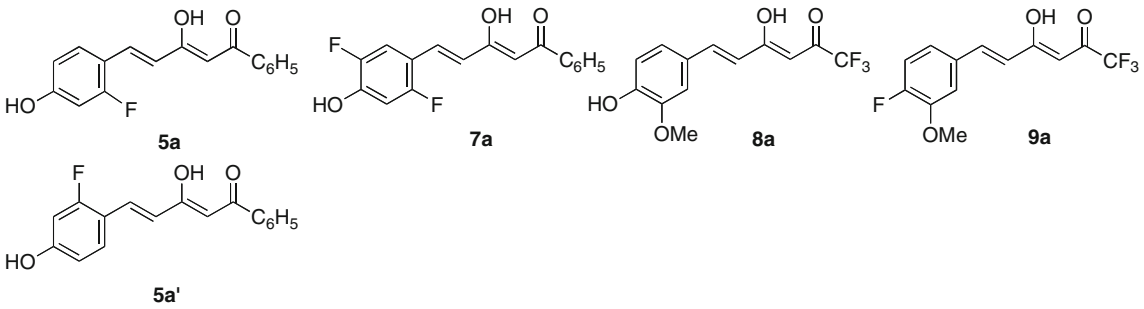

Fig. 14 Compounds studied by Quantum ESPRESSO

Table 12 Four independent molecules of compound **9**. Always the split corresponds to a 1:1 ratio

	[CP]MAS			Calc. σ PBE-crystal				
	Mol 1,2	Mol 3,4	$\lvert\Delta\delta\rvert$	Mol 1	Mol 2	Mol 3	Mol 4	$\lvert\Delta\delta\rvert$ max
$^{13}C\ CF_3$	117.3	117.3[a]	0	116.74	116.72	117.88	117.87	1.16
C1	180.1	180.1	0	180.74	180.45	179.95	179.70	1.04
C2	95.2	95.2	0	98.79	98.75	99.09	99.06	0.34
C3	181.4	181.4	0	177.94	177.84	178.59	178.51	0.75
C4	118.0	118.0	0	119.39	119.39	119.68	119.64	0.29
C5	143.2	146.2	3.0	145.43	145.39	148.29	148.31	2.92
C1′	130.9	132.1	1.2	131.94	132.12	132.88	133.04	1.10
C2′	114.1	114.1	0	117.67	117.73	117.78	117.85	0.18
C3′	146.9	146.9	0	149.29	149.18	150.08	149.96	0.90
C4′	151.7	154.0	2.3	159.46	159.35	159.83	159.72	0.48
C5′	116.0	118.0	2.0	117.47	117.27	115.19	115.02	2.45
C6′	118.0	118.0	0	118.33	118.53	118.37	118.56	0.23
OCH_3	55.7	54.6	1.1	55.03	55.08	56.86	56.89	1.86
$^{19}F\ CF_3$	−74.1	−74.1	0	−66.51	−66.49	−65.53	−65.53	0.98
F4′	−130.6	−129.3	1.3	−125.01	−125.22	−124.92	−124.92	0.30

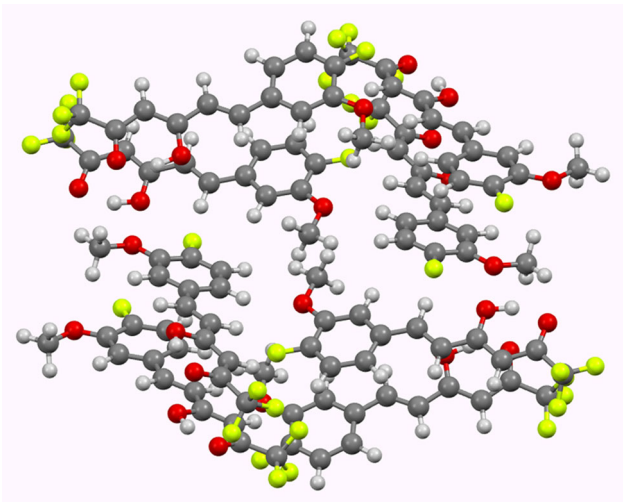

Fig. 15 Eight molecules of compound **9**

$C_{17}H_{12}F_2O_3$ (302.28): calcd. C 67.55, H 4.00; found C 67.42, H 3.94.

*(2Z,4E)-5-(2,5-difluoro-4-hydroxyphenyl)-3-hydroxy-1-phenylpenta-2,4-dien-1-one (**7**)*

1-Phenylbutane-1,3-dione (15 mmol) and boric anhydride (10.5 mmol) were mixed in dry ethyl acetate (11.25 mL) at 50 °C for 30 min. After that, a mixture of 2,5-difluoro-4-hydroxybenzaldehyde (15 mmol) and tributyl borate (22.5 mmol) in dry ethyl acetate (7.5 mL) was added, with stirring for 30 min at 50 °C. A solution of butylamine (15 mmol) in dry ethyl acetate (7.5 mL) was added slowly over 15 min. The reaction mixture was stirred at 50 °C for 90 min and then overnight at room temperature. Hydrochloric acid (1 M, 30 mL) was then added to the solution at 50 °C, and the system was stirred for 1 h. After

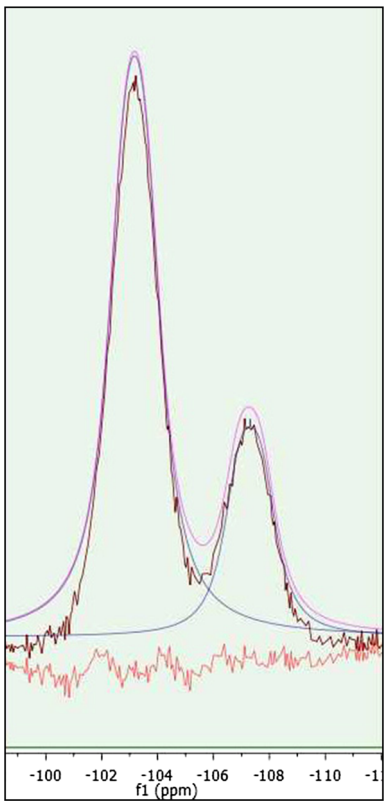

Fig. 16 ^{19}F MAS spectrum of compound **5** (a mixture of **5a** and **5a′**)

cooling, the organic layer was separated from the aqueous layer and extracted with 3 × 15 mL of ethyl acetate. The organic layer was washed with water (10 mL, 2 times) and dried (Na_2SO_4), and the solvent was evaporated under vacuum. The crude product was purified by column chromatography with dichloromethane/ethanol (95:5) as eluent, m.p. 189.8 °C (ethanol/dichloromethane) (2.99 g, yield 66 %). $C_{17}H_{12}F_2O_3$ (302.28): calcd. C 67.55, H 4.00; found C 67.64, H 4.05.

*(3Z,5E)-1,1,1-trifluoro-6-(4-fluoro-3-methoxyphenyl)-4-hydroxyhexa-3,5-dien-2-one (**9**)*

1,1,1-Trifluoropentane-2,4-dione (15 mmol) and boric anhydride (10.5 mmol) were mixed in dry ethyl acetate (11.25 mL) at 50 °C for 30 min. After that, a mixture of 4-fluoro-3-methoxybenzaldehyde (15 mmol) and tributyl borate (22.5 mmol) in dry ethyl acetate (7.5 mL) was added, with stirring for 30 min at 50 °C. A solution of butylamine (15 mmol) in dry ethyl acetate (7.5 mL) was added slowly over 15 min. The reaction mixture was stirred at 50 °C for 90 min and then overnight at room temperature. Hydrochloric acid (1 M, 30 mL) was then added to the solution at 50 °C, and the system was stirred for 1 h. After cooling, the organic layer was separated from the aqueous layer and extracted with 3 × 15 mL of ethyl acetate. The organic layer was washed with water (10 mL, 2 times) and dried (Na_2SO_4), and the solvent was evaporated under vacuum. The crude product was purified by column chromatography with ethyl acetate/hexane (30:70) as eluent, m.p. 110.8 °C (ethyl acetate/hexane) (499.7 mg, yield 11 %). $C_{13}H_{10}F_4O_3$ (290.21): calcd. C 53.80, H 3.47; found C 53.75, H 3.37.

*(3Z,5E)-1,1,1-trifluoro-6-(3-fluoro-4-hydroxyphenyl)-4-hydroxyhexa-3,5-dien-2-one (**10**)*

1,1,1-Trifluoropentane-2,4-dione (15 mmol) and boric anhydride (10.5 mmol) were mixed in dry ethyl acetate (11.25 mL) at 50 °C for 30 min. After that, a mixture of 3-fluoro-4-hydroxybenzaldehyde (15 mmol) and tributyl borate (22.5 mmol) in dry ethyl acetate (7.5 mL) was added, with stirring for 30 min at 50 °C. A solution of butylamine (15 mmol) in dry ethyl acetate (7.5 mL) was added slowly over 15 min. The reaction mixture was stirred at 50 °C for 90 min and then overnight at room temperature. Hydrochloric acid (1 M, 30 mL) was then added to the solution at 50 °C, and the system was stirred for 1 h. After cooling, the organic layer was separated from the aqueous layer and extracted with 3 × 15 mL of ethyl acetate. The organic layer was washed with water (10 mL, 2 times) and dried (Na_2SO_4), and the solvent was evaporated under vacuum. The crude product was purified by column chromatography with dichloromethane/ethanol (95:5) as eluent, m.p. 134.4 °C (ethanol/dichloromethane) (1.1 g, yield 26 %). $C_{12}H_8F_4O_3$ (276.18): calcd. C 52.19, H 2.92; found C 52.14, H 2.88.

*(3Z,5E)-1,1,1-trifluoro-6-(2-fluoro-4-hydroxyphenyl)-4-hydroxyhexa-3,5-dien-2-one (**11**)*

1,1,1-Trifluoropentane-2,4-dione (15 mmol) and boric anhydride (10.5 mmol) were mixed in dry ethyl acetate (11.25 mL) at 50 °C for 30 min. After that, a mixture of 2-fluoro-4-hydroxybenzaldehyde (15 mmol) and tributyl borate (22.5 mmol) in dry ethyl acetate (7.5 mL) was added, with stirring for 30 min at 50 °C. A solution of butylamine (15 mmol) in dry ethyl acetate (7.5 mL) was added slowly over 15 min. The reaction mixture was stirred at 50 °C for 90 min and then overnight at room temperature. Hydrochloric acid (1 M, 30 mL) was then added to the solution at 50 °C, and the system was stirred for 1 h. After cooling, the organic layer was separated from the aqueous layer and extracted with 3 × 15 mL of ethyl acetate. The organic layer was washed with water (10 mL, 2 times) and dried (Na_2SO_4), and the solvent was evaporated under vacuum. The crude product was purified by column chromatography with dichloromethane/ethanol (95:5) as eluent, m.p. 151.2 °C (ethanol/dichloromethane)

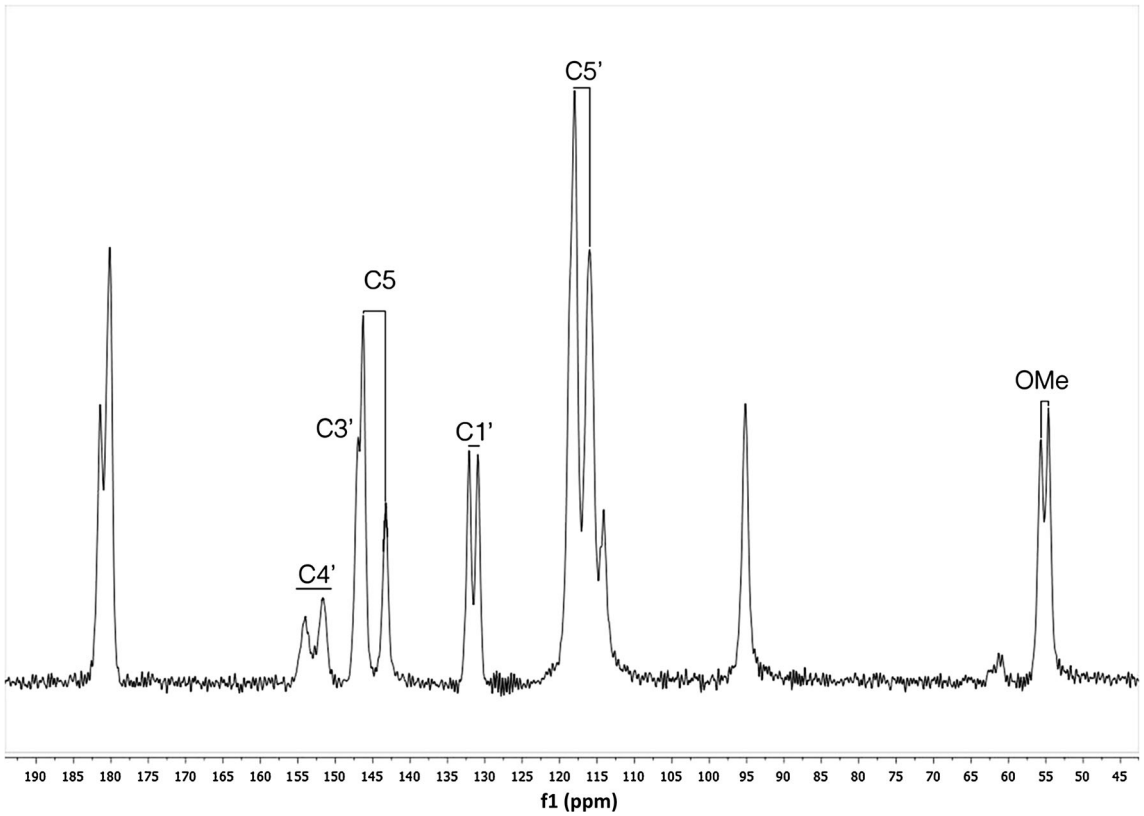

Fig. 17 ^{13}C CPMAS NMR spectrum of (3*Z*,5*E*)-1,1,1-trifluoro-6-(4-fluoro-3-methoxyphenyl)-4-hydroxyhexa-3,5-dien-2-one (**9**). Split signals, C4′, C5, C1′, C5′ and OMe are identified

(1.35 g, yield 33 %). $C_{12}H_8F_4O_3$ (276.18): calcd. C 52.19, H 2.92; found C 52.08, H 3.09.

*(3Z,5E)-6-(2,4-difluoro-3-hydroxyphenyl)-1,1,1-trifluoro-4-hydroxyhexa-3,5-dien-2-one (**12**)*

1,1,1-Trifluoropentane-2,4-dione (15 mmol) and boric anhydride (10.5 mmol) were mixed in dry ethyl acetate (11.25 mL) at 50 °C for 30 min. After that, a mixture of 2,4-difluoro-3-hydroxybenzaldehyde (15 mmol) and tributyl borate (22.5 mmol) in dry ethyl acetate (7.5 mL) was added, with stirring for 30 min at 50 °C. A solution of butylamine (15 mmol) in dry ethyl acetate (7.5 mL) was added slowly over 15 min. The reaction mixture was stirred at 50 °C for 90 min and then overnight at room temperature. Hydrochloric acid (1 M, 30 mL) was then added to the solution at 50 °C, and the system was stirred for 1 h. After cooling, the organic layer was separated from the aqueous layer and extracted with 3 × 15 mL of ethyl acetate. The organic layer was washed with water (10 mL, 2 times) and dried (Na_2SO_4), and the solvent was evaporated under vacuum. The crude product was purified by column chromatography with dichloromethane/ethanol (95:5) as eluent, m.p. 129.1 °C (ethanol/dichloromethane) (733.12 mg, yield 17 %). $C_{12}H_7F_5O_3$ (294.18): calcd. C 48.99, H 2.40; found C 49.28, H 2.66.

*(3Z,5E)-6-(2,5-difluoro-4-hydroxyphenyl)-1,1,1-trifluoro-4-hydroxyhexa-3,5-dien-2-one (**13**)*

1,1,1-Trifluoropentane-2,4-dione (15 mmol) and boric anhydride (10.5 mmol) were mixed in dry ethyl acetate (11.25 mL) at 50 °C for 30 min. After that, a mixture of 2,5-difluoro-3-hydroxybenzaldehyde (15 mmol) and tributyl borate (22.5 mmol) in dry ethyl acetate (7.5 mL) was added, with stirring for 30 min at 50 °C. A solution of butylamine (15 mmol) in dry ethyl acetate (7.5 mL) was added slowly over 15 min. The reaction mixture was stirred at 50 °C for 90 min and then overnight at room temperature. Hydrochloric acid (1 M, 30 mL) was then added to the solution at 50 °C, and the system was stirred for 1 h. After cooling, the organic layer was separated from the aqueous layer and extracted with 3 × 15 mL of ethyl acetate. The organic layer was washed with water (10 mL, 2 times) and dried (Na_2SO_4), and the solvent was evaporated under vacuum. The crude product was purified by column chromatography with ethyl acetate/hexane (80:20) as eluent, m.p. 190.8 °C (ethanol/dichloromethane)

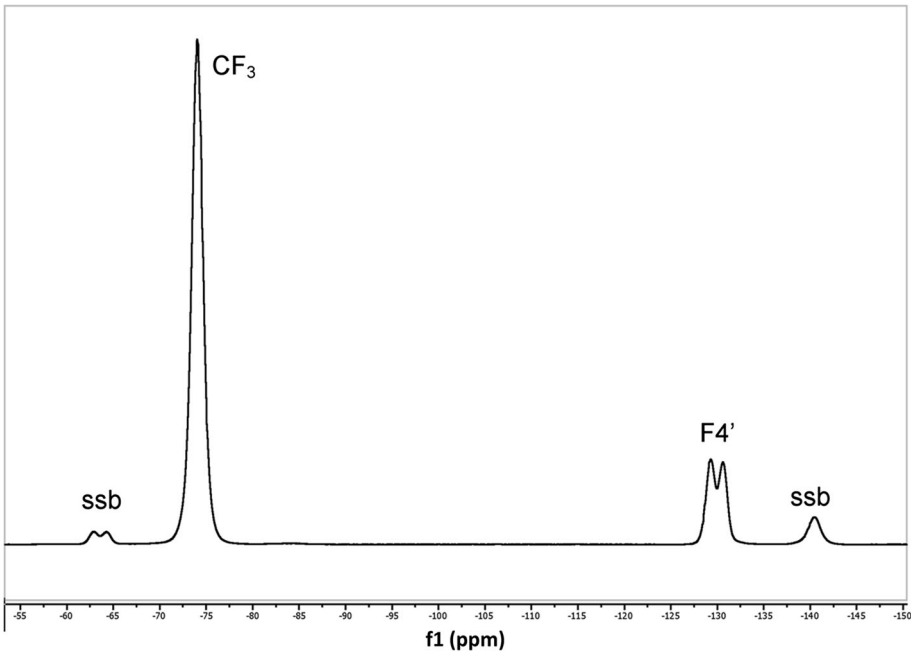

Fig. 18 ^{19}F MAS NMR spectrum of compound **9**

(900 mg, yield 20 %). $C_{12}H_7F_5O_3$ (294.18): calcd. C 48.99, H 2.40; found C 48.82, H 2.36.

Computational details

The geometry of the molecules has been fully optimized with the hybrid HF/DFT B3LYP computational method and the B3LYP/6-311 ++G(d,p) level [28, 29]. Frequency calculations have been carried out at the same computational level to verify that the structures obtained correspond to energetic minima. These geometries have been used for the calculations of the absolute chemical shieldings with the GIAO method [30, 31]. All the calculations have been carried out with the Gaussian-09 package [32]. Equations 18–20 have been used to transform absolute shieldings into chemical shifts [33–35]:

$$\delta^1\mathrm{H} = 31.0 - 0.97 * \sigma^1\mathrm{H}, \text{ (reference TMS, 0.00 ppm)} \quad (18)$$

$$\delta^{13}\mathrm{C} = 175.7 - 0.963 * \sigma^{13}\mathrm{C}, \text{ (reference TMS, 0.00 ppm)} \quad (19)$$

$$\delta^{19}\mathrm{F} = 162.1 - 0.959 * \sigma^{19}\mathrm{F}, \text{ (reference } CFCl_3\text{, 0.00 ppm)} \quad (20)$$

Quantum ESPRESSO (QE) [36] was employed to optimize the crystal structures starting from the experimental geometries, one already published (UFIMON [11–13]) and the others reported at the experimental section, using DFT-D [37, 38]. The DFT gauge-including projector augmented wave (GIPAW [39]) method with pseudopotentials to approximate the core electron wavefunction, as implemented in the program Quantum ESPRESSO, is used to predict the complete ^{13}C and ^{19}F chemical shift tensors for all carbons and fluorine, for crystal and isolated configuration, at the PBE level of theory [40, 41]. We have successfully employed QE in previous papers [42, 43]. The transformation of these calculated absolute shieldings (σ, ppm) into chemical shifts (δ, ppm) will be discussed below (Table 12).

The parameters employed to make QE calculations were set to achieve convergence in the self consistent field (SCF) energy. The details of their selection are the following. (1) The DFT-D pseudopotentials from www.quantum-espresso.org are the ultrasoft pbe-rrjkus-gipaw-dc and were tested for every calculation. (2) The convergence of the SCF calculations, *conv*, was varied from 10^{-7} to 10^{-12} and set in 10^{-10}. (3) The energy cutoff for the wavefunction, *ecutwfc*, was varied between 35 and 95 and set in 65, corresponding to the minimum number of plane waves to achieve SCF energy convergence. (4) The k points were varied between 1 and 4 in each dimension and set in $k = 2$, employing again the criteria of reaching the minimum SCF energy. All calculations were performed using version 5.0.1 of QE. Calculations were performed on four-core nodes (Intel I5 processors, 3.0 GHz) with 16 GB RAM.

Compound **5** that shows a 70 % **5a**–30 % **5a**′ disorder involving the fluorine substituent and 4 molecules in the unit cell has been approximated calculating independently a unit cell with four **5a** molecules and another unit cell containing four **5a**′ molecules.

In the case of compound **5** (a mixture of **5a** and **5a**′), we have also carried out CASTEP calculations [44]. Geometry

optimizations of crystals **5a** and **5a′** were performed using the GGA(PBE) [40, 41] exchange correlation functional and the Grimme dispersion correction [37, 38]. A plane wave kinetic cutoff energy of 66.1 Ry, 2*k* points and total energy, force, displacement, and stress convergence tolerances of 5×10^{-6} eV, 10^{-1} eV Å^{-1}, 5×10^{-4} Å and 2×10^{-1} GPa, respectively, were employed. These settings were also used for the calculation of NMR parameters [45, 46].

Single-crystal X-ray analysis

Data collection for **5** and **9** was carried out at room temperature on a Bruker Smart CCD diffractometer and on a Xcalibur Atlas CCD diffractometer, also at room temperature, for **7**, using in all cases graphite-monochromated Mo-Kα radiation ($\lambda = 0.71073$ Å) operating at 50 kV and 35 mA for **5** and **9** and at 50 kV and 40 mA for **7**. The exposure times were 20 s for **5** and **9** and 35 s for **7** in omega. A summary of the fundamental crystal and refinement data is given in Table 13.

The structures were solved by direct methods and refined by full-matrix least-squares procedures on F^2 (SHELXL-97) [47]. All non-hydrogen atoms were refined anisotropically. The hydrogen atoms were included in their calculated positions and refined riding on the respective carbon atoms with the exception of hydrogens H3A bonded to O3 for **5**, H3A and H3B bonded to O3A and O3B, respectively, for **7** and **9** that were located in a Fourier synthesis and refined riding on the respective bonded atoms. For compound **5**, the fluorine atom is disordered on C6 (F6 with 70 % occupancy) and on C2 (F6′ with 30 % occupancy). Note that the numbering used in the crystallographic analysis differs from the standard one used for naming the compounds and for the NMR part. For compound **5**, if otherwise not stated, the fluorine atom will be placed at position 6 (crystallography), i.e., position 2′ of Fig. 3.

CCDC 1407607-1407609 contains the supplementary crystallographic data for this paper. These data can be obtained free of charge from The Cambridge Crystallographic Data Centre via www.ccdc.cam.ac.uk/data_request/cif.

Table 13 Crystal and refinement data for **5**, **7** and **9**

Crystal data	**5**	**7**	**9**
Empirical formula	$C_{17}H_{13}F_1O_3$	$C_{17}H_{12}F_2O_3$	$C_{13}H_{10}F_4O_3$
Formula wt	284.27	302.27	290.21
Crystal system	Orthorhombic	Orthorhombic	Monoclinic
Space group	$Pna2_1$	$Pna2_1$	$P2_1/n$
a/Å	21.459(6)	20.622(2)	7.557(1)
b/Å	12.065(4)	11.917(2)	24.756(4)
c/Å	5.433(2)	5.6096(6)	13.730(2)
α/°	90	90	90
β/°	90	90	94.078(3)
γ/°	90	90	90
V/Å^3	1406.6(7)	1378.6(3)	2562.2(7)
Z	4	4	8
D_c/g/cm^3	1.342	1.456	1.505
μ(Mo–Ka)/mm^{-1}	0.100	0.117	0.143
F(000)	592	624	1184
q range/°	1.90–25.01	3.42–25.01	1.65–26.01
Index ranges	−25, −13, −6 to 23, 14, 6	−24, −11, −6 to 18, 14, 5	−9, −30, −16 to 9, 30, 13
Reflections collected	10,375	4206	21,061
Unique reflections [*R*(int)]	2472[*R*(int) = 0.0593]	1897 [*R*(int) = 0.0379]	5030 [*R*(int) = 0.0802]
Completeness to theta	99.9 %	99.8 %	99.9 %
Data/restraints/parameters	2472/1/188	1897/1/199	5030/0/361
Goodness of fit on F^2	0.993	0.996	0.998
*R*1 (reflns obs) [$I > 2\sigma(I)$][a]	0.0450 (1205)	0.0486 (1265)	0.0523 (2194)
*wR*2 (all data)[b]	0.1133	0.1335	0.1689

[a] $R1 = \Sigma||F_o| - |F_c||/\Sigma|F_o|$

[b] $wR2 = \{\Sigma[w(F_o^2 - F_c^2)^2]/\Sigma[w(F_o^2)^2]\}$

NMR parameters

Solution NMR spectra (in $CDCl_3$, DMSO-d_6 or in a $CDCl_3$/DMSO-d_6 mixture depending on the solubility of the compounds) were recorded on a Bruker DRX 400 (9.4 Tesla, 400.13 MHz for ^1H, 100.62 MHz for ^{13}C, and 376.50 MHz for ^{19}F) spectrometer with a 5-mm inverse-detection H–X probe equipped with a z-gradient coil (^1H, ^{13}C) and with a QNP 5-mm probe (^{19}F), at 300 K. Chemical shifts (δ in ppm) are given from internal solvent, DMSO-d_6 2.49 for ^1H and 39.5 for ^{13}C, $CDCl_3$ 7.26 for ^1H and 77.0 for ^{13}C. $CFCl_3$ was used as an external reference for ^{19}F. Coupling constants (J in Hz) are accurate to ± 0.2 Hz for ^1H, ± 0.8 Hz for ^{19}F and ± 0.6 Hz for ^{13}C. Typical parameters for ^1H NMR spectra were spectral width 7000 Hz and pulse width 7.5 μs at an attenuation level of 0 dB. Typical parameters for ^{19}F NMR spectra were spectral width 55 kHz, pulse width 13.75 μs at an attenuation level of −6 dB and relaxation delay 1 s. Typical parameters for ^{13}C NMR spectra were spectral width 21 kHz, pulse width 10.6 μs at an attenuation level of −6 dB and relaxation delay 2 s; WALTZ-16 was used for broadband proton decoupling; the FIDs were multiplied by an exponential weighting (lb = 2 Hz) before Fourier transformation. 2D (^1H–^{13}C) gs-HMQC and (^1H–^{13}C) gs-HMBC were acquired and processed using standard Bruker NMR software and in non-phase-sensitive mode [48]. Gradient selection was achieved through a 5 % sine-truncated-shaped pulse gradient of 1 ms. Selected parameters for (^1H–^{13}C) gs-HMQC and gs-HMBC spectra were spectral width 3500 Hz for ^1H and 20.5 kHz for ^{13}C, 1024 × 256 data set, number of scans 2 (gs-HMQC) or 4 (gs-HMBC) and relaxation delay 1 s. The FIDs were processed using zero filling in the $F1$ domain, and a sine-bell window function in both dimensions was applied prior to Fourier transformation. In the gs-HMQC experiments, GARP modulation of ^{13}C was used for decoupling.

Solid-state ^{13}C (100.73 MHz) CPMAS NMR spectra have been obtained on a Bruker WB 400 spectrometer at 300 K using a 4-mm DVT probehead. Samples were carefully packed in a 4-mm-diameter cylindrical zirconia rotor with Kel-F end caps. Operating conditions involved 3.2-μs 90° ^1H pulses and decoupling field strength of 86.2 kHz by TPPM sequence. ^{13}C spectra were originally referenced to a glycine sample, and then the chemical shifts were recalculated to the Me_4Si [for the carbonyl atom δ (glycine) = 176.1 ppm]. Typical acquisition parameters for ^{13}C CPMAS were: spectral width, 40 kHz; recycle delay, 5–160 s; acquisition time, 30 ms; contact time, 30 ms; and spin rate, 12 kHz. In order to distinguish protonated and unprotonated carbon atoms, the NQS (non-quaternary suppression) experiment by conventional cross-polarization was recorded, before the acquisition the decoupler is switched off for a very short time of 25 μs [49–51].

Solid-state ^{19}F (376.94 MHz) NMR spectra have been obtained on a Bruker WB 400 spectrometer using a MAS DVT BL2.5 X/F/H double-resonance probehead. Samples were carefully packed in 2.5-mm-diameter cylindrical zirconia rotors with Kel-F end caps. Samples were spun at the magic angle at rates of 25 kHz, and the experiments were carried out at ambient probe temperature.

The typical acquisition parameters $^{19}F\{^1H\}$ MAS were: spectral width, 75 kHz; recycle delay, 10 s; pulse width, 2.5 μs and proton decoupling field strength of 100 kHz by SPINAL-64 sequence; recycle delay, 10 s; acquisition time, 25 ms; 128 scans; and spin rate, 25 kHz. The ^{19}F spectra were referenced to ammonium trifluoroacetate sample, and then, the chemical shifts were recalculated to the $CFCl_3$ (δ $CF_3CO_2^-$ NH_4^+ = −72.0 ppm).

Conclusions

1. The fact that two independent methods, one based on geometries optimized in the gas phase (perturbed or not by a solvent) and the other based on the experimental geometries of the crystal (including the surrounding molecules), lead to highly proportional absolute shieldings indicates that solid-state chemical shifts can be assigned based on GIAO/B3LYP/6-311 ++G(d,p) calculations including DMSO solvent effects, as a continuum. It is as DMSO could mimic the crystal field effects.
2. Since QE uses experimental geometries, we can exclude that the solid-state chemical shifts correspond to a rapid equilibrium between **a** and **b** tautomers.
3. Even if GIAO/DMSO calculations are a good approximation to solid-state (CPMAS and MAS) chemical shifts, this approach cannot justify the splittings that QE calculations account in a satisfactory way.
4. It is highly satisfying that for compound **5**, the results concerning the two rotamers, **5a** and **5a′**, are homogeneous: ^{19}F MAS NMR, 74 % of **5a** and 26 % of **5a′** (this allow to assign the signal at −103.2 ppm to **5a** and that at −107.3 ppm to **5a′**); X-ray crystallography, 70 % of **5a** and 30 % of **5a′**; theoretical calculations, 66.5 % of **5a** and 33.5 % of **5a′**. In contrast, in DMSO-d_6 solution, there are (32 ± 18) % of **5a** and (68 ± 18) % of **5a′**, an inversion we assigned to the higher dipole moment of the latter.

Acknowledgments This work has been financed by Ministerio de Economía y Competitividad of Spain (CTQ2012-35513-C02-02 and CTQ2014-56833-R) and Comunidad Autónoma de Madrid (Project Fotocarbon, S2013/MIT-2841). One of us (C. I. Nieto) is indebted to

UNED for a predoctoral fellowship (FPI "Grupos de Investigación" UNED). Financial support from the Universidad de Buenos Aires and the CONICET is also greatly acknowledged.

References

1. Aggarwal BB, Bhatt ID, Ichikawa H, Ahn KS, Sethi G, Sandur KS, Sundaram C, Seeram N, Shishodia S (2007) Curcumin: biological and medicinal properties. Turmeric the genus curcuma, chapter 10, vol 45. CRC Press, New York, pp 279–369
2. Anand P, Thomas SG, Kunnumakkara AB, Sundaram C, Harikumar KB, Sung B, Tharakan ST, Misra K, Priyadarsini IK, Rajasekharan KN, Aggarwal BB (2008) Biochem Pharmacol 76:1590–1611
3. Itokawa H, Shi Q, Toshiyuki A, Morris-Natschke SL, Lee KH (2008) Chin Med 3:11–23
4. Subash C, Sridevi P, Wonil K, Bharat BA (2012) Clin Exp Pharmacol Physiol 39:283–299
5. Bukhari SNA, Jantan IB, Jasamai M, Ahmad W, Amjad MWB (2013) J Med Sci 13:501–513
6. Prasad S, Gupta SC, Tyagi AK, Aggarwal BB (2014) Biotecnol Adv 32:1053–1064
7. Shanmugam MK, Rane G, Kanchi MM, Arfuso F, Chinnathambi A, Zayed ME, Alharbi SA, Tan BKH, Kumar AP, Sethi G (2015) Molecules 20:2728–2769
8. Cornago P, Claramunt RM, Bouissane L, Alkorta I, Elguero J (2008) Tetrahedron 64:8089–8094
9. Claramunt RM, Bouissane L, Cabildo P, Cornago P, Elguero J, Radziwon A, Medina C (2009) Bioorg Med Chem 17:1290–1296
10. Cornago P, Cabildo P, Sanz D, Claramunt RM, Torralba MC, Torres MR, Elguero J (2013) Eur J Org Chem, 6043–6054
11. CSD database version 5.33 (2008) updates (Nov. 2011)
12. Allen FH (2002) Acta Crystallogr Sect B 58:380–388
13. Allen FH, Motherwell WDS (2002) Acta Crystallogr Sect B 58:407–422, http://www.ccdc.cam.ac.uk
14. Kubinyi H (1988) QSAR 7:121–133
15. Alkorta I, Blanco F, Elguero J (2008) Tetrahedron 64:3826–3836
16. Iglesias-Sánchez JC, María DS, Claramunt RM, Elguero J (2010) Molecules 15:1213–1222
17. Sloop JC (2013) Rep Org Chem 3:1–12
18. Grage SL, Dürr UHN, Afonin S, Mikhailiuk PK, Komarov IV, Ulrich AS (2008) J Magn Reson 191:16–23
19. Anisotropic displacement parameters, www.iucr.org/comm/cnom/adp/finrep/node8.html
20. Kumar R, Fronczek FR, Maverick AW, Kim AJ, Butler LG (1994) Chem Mater 6:587–595
21. Wang X, Mallory FB, Mallory CW, Beckmann PA, Rheingold AL, Francl MM (2006) J Phys Chem A 110:3954–3960
22. Chandrappa RK, Ochsenbein P, Martineau C, Bonin M, Althoff G, Engelke F, Malandrini H, Castro B, Hajji ME, Taulelle F (2013) Cryst Growth Des 13:4678–4687
23. Alkorta I, Elguero J, Pérez-Torralba M, López C, Claramunt RM (2015) Magn Reson Chem 53:353–362
24. Uldry AC, Griffin JM, Yates JR, Pérez-Torralba M, María MDS, Webber AL, Beaumont M, Samoson A, Claramunt RM, Pickard CJ, Brown SP (2008) J Am Chem Soc 130:945–954
25. Webber AL, Emsley L, Claramunt RM, Brown SP (2010) J Phys Chem 114:10435–10442
26. Di Fiori N, Orendt AM, Caputo MC, Ferraro MB, Facelli JC (2004) Magn Reson Chem 42:S41–S47
27. Nieto CI, Cabildo P, García MA, Claramunt RM, Alkorta I, Elguero J (2014) Beilstein J Org Chem 10:1620–1629
28. Ditchfield R, Hehre WJ, Pople JA (1971) J Chem Phys 54:724–728
29. Frisch MJ, Pople JA, Binkley JS (1984) J Chem Phys 80:3265–3269
30. Ditchfield R (1974) Mol Phys 27:789–807
31. London F (1937) J Phys Radium 8:397–409
32. Frisch MJ, Trucks GW, Schlegel HB, Scuseria GE, Robb MA, Cheeseman JR, Scalmani G, Barone V, Mennucci B, Petersson GA, Nakatsuji H, Caricato M, Li X, Hratchian HP, Izmaylov AF, Bloino J, Zheng G, Sonnenberg JL, Hada M, Ehara M, Toyota K, Fukuda R, Hasegawa J, Ishida M, Nakajima T, Honda Y, Kitao O, Nakai H, Vreven T, Montgomery JA Jr, Peralta JE, Ogliaro F, Bearpark M, Heyd JJ, Brothers E, Kudin KN, Staroverov VN, Kobayashi R, Normand J, Raghavachari K, Rendell A, Burant JC, Iyengar SS, Tomasi J, Cossi M, Rega N, Millam NJ, Klene M, Knox JE, Cross JB, Bakken V, Adamo C, Jaramillo J, Gomperts R, Stratmann RE, Yazyev O, Austin AJ, Cammi R, Pomelli C, Ochterski JW, Martin RL, Morokuma K, Zakrzewski VG, Voth GA, Salvador P, Dannenberg JJ, Dapprich S, Daniels AD, Farkas Ö, Foresman JB, Ortiz JV, Cioslowski J, Fox DJ (2009) Gaussian 09, Revision A. 1. Gaussian, Inc., Wallingford
33. Silva AMS, Sousa RMS, Jimeno ML, Blanco F, Alkorta I, Elguero J (2008) Magn Reson Chem 46:859–864
34. Blanco F, Alkorta I, Elguero J (2007) Magn Reson Chem 45:797–800
35. Fresno N, Pérez-Fernández R, Jimeno ML, Alkorta I, Sánchez-Sanz G, Elguero J, Del Bene JE (2012) J Heterocycl Chem 49:1257–1259
36. Giannozzi P, Baroni S, Bonini N, Calandra M, Car R, Cavazzoni C, Ceresoli D, Chiarotti GL, Cococcioni M, Dabo I, Dal Corso A, Fabris S, Fratesi G, de Gironcoli S, Gebauer R, Gerstmann U, Gougoussis C, Kokalj A, Lazzeri M, Martin-Samos L, Marzari N, Mauri F, Mazzarello R, Paolini S, Pasquarello A, Paulatto L, Sbraccia C, Scandolo S, Sclauzero G, Seitsonen AP, Smogunov A, Umari P, Wentzcovitch RM (2009) J Phys Condens Matter 21:395502–395519, http://www-quantum-espresso.org
37. Grimme S (2004) J Comput Chem 25:1463–1473
38. Grimme S (2006) J Comput Chem 27:1787–1799
39. Bonhomme C, Gervais C, Babonneau F, Coelho C, Pourpoint F, Azaïs T, Ashbrook SE, Griffin JM, Yates JR, Mauri F, Pickard CJ (2012) Chem Rev 112:5733–5779
40. Perdew JP, Burke K, Ernzerhof M (1996) Phys Rev Lett 77:3865–3868
41. Perdew JP, Burke K, Wang Y (1996) Phys Rev B 54:16533–16539
42. Silva AMS, Silva VLM, Claramunt RM, María DS, Ferraro MB, Reviriego F, Alkorta I, Elguero J (2013) Magn Reson Chem 51:530–540
43. Alkorta I, Claramunt RM, Elguero J, Ferraro MB, Facelli JC, Provasi PF, Reviriego F (2014) J Mol Struct 107:551–558
44. Clark SJ, Segall MD, Pickard CJ, Hasnip PJ, Probert MJ, Refson K, Payne MC (2005) Z Krist 220:567–570
45. Pickard CJ, Mauri F (2001) Phys Rev B 63:245101
46. Yates JR, Pickard CJ, Mauri F (2007) Phys Rev B 76:024401
47. Sheldrick GM (1997) SHELX97, program for refinement of crystal structure. University of Göttingen, Göttingen
48. Berger S, Braun S (2004) 200 and more NMR experiments. Wiley, Weinheim
49. Murphy PD (1983) J Magn Reson 52:343–345
50. Murphy PD (1985) J Magn Reson 62:303–308
51. Alemany LB, Grant DM, Alger TD, Pugmire RJ (1983) J Am Chem Soc 105:669–6704